Green's functions for transversely isotropic piezoelectric functionally graded multilayered half spaces

E. Pan [*], F. Han

Department of Civil Engineering, University of Akron, Akron, OH 44325-3905, USA

Abstract

By virtue of two systems of vector functions and the propagator matrix method, Green's functions for transversely isotropic, piezoelectric functionally graded (exponentially graded in the vertical direction), and multilayered half spaces are derived. It is observed that the homogeneous solution and propagator matrices for each functionally graded layer in the transformed domain are independent of the choice of the two systems of vector functions. For a point force and point charge density applied at any location of the functionally graded half space, Green's functions are expressed in terms of one-dimensional infinite integrals. To carry out the numerical integral involving Bessel functions, an adaptive Gauss quadrature approach is introduced and modified. The piezoelectric functionally graded Green's functions include those in the corresponding elastic functionally graded media as special results with the latter being also unavailable in the literature. Two piezoelectric functionally graded half-space models are analyzed numerically: one is a functionally graded PZT-4 half space, and the other a coated functionally graded PZT-4 layer over a homogeneous $BaTiO_3$ half space. The effects of different exponential factors on Green's function components are clearly demonstrated, which could be useful in the design and manufacturing of piezoelectric functionally graded structures.
© 2004 Elsevier Ltd. All rights reserved.

Keywords: Transverse isotropy; Functionally graded material (FGM); Piezoelectric material; Green's function; Multilayered structure; Systems of vector functions; Propagator matrix method

1. Introduction

With spatial variation in their compositions, functionally graded materials (FGMs) can be utilized to provide the desirable thermo-mechanical, piezoelectric, and magnetic properties. As such, applications of

[*] Corresponding author. Tel.: +1 330 972 6739; fax: +1 330 972 6020.
E-mail address: pan2@uakron.edu (E. Pan).

FGMs can be in very diverse disciplines such as tribology, electronics, and biomechanics (Hirai, 1995; Markworth et al., 1995; Suresh and Mortensen, 1998; Miyamoto et al., 1999; Rodel, 2003). While the thermomechanical application of FGM is well known in thermal barrier coatings (e.g., Jarvis and Carter, 2002), that related to piezoelectricity is currently being explored (Xu et al., 1999; Almajid and Taya, 2001; Almajid et al., 2001). Recent preliminary results on fabrication of piezoelectric FGM (PFGM) mono-morph, biomorph, and related piezodevices (Almajid and Taya, 2001; Almajid et al., 2001; Chen and Ma, 2002; Rodel, 2003) have shown clearly the benefit of using PFGMs. Furthermore, couplings among different phases (electric, mechanical, and even magnetic) are the key factors for future smart, adaptive, and functional materials and structures (e.g., Dunn and Taya, 1993; Yang and Tiersten, 1997; Newnham and Amin, 1999).

The special feature of graded spatial compositions associated with FGMs provides freedom in the design and manufacturing of novel structures; on the other hand, it poses great challenges in numerical modeling and simulation of the FGM structure. For example, to apply the domain-discretization method (e.g., the finite element), one may need to develop special elements (Kim and Paulino, 2002a,b, 2003; Santare et al., 2003; Liew et al., 2003). This could be difficult for the three-dimensional (3D) problem involving FGMs, but can be extremely useful to complex FGM analysis.

Alternatively, one can employ the boundary element method (BEM) to attack the problems associated with FGMs. The BEM has the advantage of boundary discretization only; however, it requires that Green's functions for the corresponding FGMs be available. For isotropic elastic FGMs, Giannakopoulos and Suresh (1997, 1999) derived the surface Green's functions due to a vertical point force applied on the surface of the half space. Recently, Martin et al. (2002) and Chan et al. (2004) obtained the analytical expressions for Green's functions in both 3D and 2D anisotropic elastic FGMs where the material prop-erties vary exponentially in a fixed direction, whilst Wang et al. (2003) solved the symmetric problem of a vertical point force in a transversely isotropic FGM half space. Certain thermal and heat conduction problems in FGM media have been also solved using the BEM method (Sutradhar et al., 2002; Gray et al., 2003; Berger et al., in press). To the best of the authors' knowledge, however, no Green's function has been derived so far for a layered elastic FGM, not to mention Green's function for the corresponding PFGM.

This paper is therefore to derive the 3D Green's functions for multilayered and transversely isotropic PFGM half spaces. First, by virtue of the Cartesian and cylindrical systems of vector functions and the propagator matrix method (Gilbert and Backus, 1966; Pan, 1989a,b; Pan, 1997), we obtain the layer solu-tion and propagator matrices in the transformed domain, which are independent of the systems of vector functions. Then, we propose a propagating approach so that the propagator matrices can be multiplied di-rectly and efficiently. Finally, we calculate the physical-domain Green's functions by introducing and mod-ifying an adaptive Gauss quadrature (Chave, 1983; Lucas, 1995). Green's functions presented in this paper include those for the corresponding elastic FGM media as special results. This paper is organized as fol-lows: In Section 2, we state the problem and the governing equations. In Section 3, the general layer solu-tion and propagator matrices are derived in the transformed domain. While the source functions are given in Section 4, Section 5 presents Green's functions in the transformed domain. In Section 6, integration issue is discussed on obtaining the physical-domain Green's functions. Numerical examples are provided in Section 7 and conclusions are drawn in Section 8.

2. Problem statement and governing equations

Let us consider a structure made up of p parallel, transversely isotropic PFGM layers lying over a trans-versely isotropic PFGM half space. The layers are numbered serially with the layer at the top being layer 1 and the last layer p, which is just above the half space (Fig. 1). We assume that in each layer the PFGM has
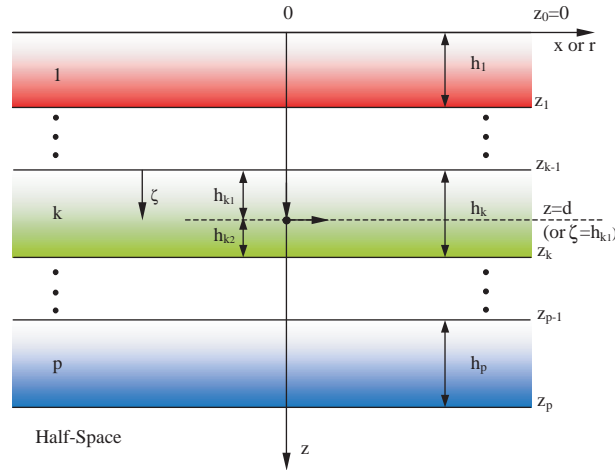
Fig. 1. Geometry of a PFGM multilayered half space. Both vertical global (z) and local (ζ) coordinates are attached to the layered half space.

a locally varied microstructure and follows an exponential variation in the vertical direction, i.e., $e^{\eta\zeta}$, where ζ is the local vertical coordinate (Fig. 1). While the exponential factor $\eta = 0$ reduces to the homogeneous material case, different variations in the vertical direction can be approximated using different exponential functions (i.e., with different η). Furthermore, for convenience of derivation, we employ two sets of coordinates in the paper. We place the global Cartesian and/or cylindrical coordinates on the surface with the z-axis pointing into the layered half space. The kth layer is bounded by the interfaces $z = z_{k-1}$, z_k. As such, z_{k-1} is the coordinate of the upper interface of the kth layer, and z_k that of the lower interface. It is obvious that $z_0 = 0$ and $z_p = H$, where H is the depth of the last layer interface. In each layer, we also place a local vertical coordinate ζ (Fig. 1 for the kth layer), with the starting point at the upper interface of the layer. Thus, the local coordinate ζ can be treated as the distance from the upper interface of the layer. Obviously, for the kth layer with a thickness h_k, the relation between the local and global coordinates is $\zeta = z - z_{k-1}$ ($0 \leqslant \zeta \leqslant h_k$).

For transversely isotropic PFGMs, we have in each layer, the following governing equations: [1]

(1) Equilibrium equations

$$\sigma_{ij,j} + f_i = 0, \tag{2.1}$$

$$D_{i,i} - q = 0, \tag{2.2}$$

where σ_{ij} and D_i are the stress and electric displacement, respectively; f_i and q are the body force and electric charge density, which will be replaced later on by a concentrated force and point charge density. In this paper, summation over repeated subscripts is implied, with a subscript comma denoting partial differentiation with respect to the coordinates (i.e., $x_1 = x$, $x_2 = y$, $x_3 = z$).

---

[1] We choose the Cartesian system of vector functions; the results in the corresponding cylindrical system of vector functions are given in Appendix A.

(2) Constitutive relations

$$\sigma_{xx} = C_{11}\gamma_{xx} + C_{12}\gamma_{yy} + C_{13}\gamma_{zz} - e_{31}E_z,$$

$$\sigma_{yy} = C_{12}\gamma_{xx} + C_{11}\gamma_{yy} + C_{13}\gamma_{zz} - e_{31}E_z,$$

$$\sigma_{zz} = C_{13}\gamma_{xx} + C_{13}\gamma_{yy} + C_{33}\gamma_{zz} - e_{33}E_z,$$

$$\sigma_{yz} = 2C_{44}\gamma_{yz} - e_{15}E_y, \tag{2.3}$$

$$\sigma_{xz} = 2C_{44}\gamma_{xz} - e_{15}E_x,$$

$$\sigma_{xy} = 2C_{66}\gamma_{xy},$$

$$D_x = 2e_{15}\gamma_{xz} + \varepsilon_{11}E_x,$$

$$D_y = 2e_{15}\gamma_{yz} + \varepsilon_{11}E_y, \tag{2.4}$$

$$D_z = e_{31}(\gamma_{xx} + \gamma_{yy}) + e_{33}\gamma_{zz} + \varepsilon_{33}E_z,$$

where γ_{ij} is the elastic strain and E_i the electric field; C_{ij}, e_{ij} and ε_{ij} are the elastic moduli, piezoelectric coefficients, and dielectric coefficients, respectively. We remark that the solutions derived in this paper include those for the corresponding elastic FGM media as a special case (by setting the piezoelectric coefficients e_{ij} to zero).

(3) Elastic displacement–strain and electric potential–electric field relations

$$\gamma_{ij} = 0.5(u_{i,j} + u_{j,i}), \tag{2.5}$$

$$E_i = -\phi_{,i}, \tag{2.6}$$

where u_i and ϕ are the elastic displacement and electric potential, respectively.

For each PFGM layer with an exponential variation in the z- (or ζ-) direction, the material coefficients in Eq. (2.3) can be described by

$$C_{ik}(\zeta) = C_{ik}^0 e^{\eta\zeta}; \quad \varepsilon_{ik}(\zeta) = \varepsilon_{ik}^0 e^{\eta\zeta}; \quad e_{ik}(\zeta) = e_{ik}^0 e^{\eta\zeta}, \tag{2.7}$$

where η is the exponential factor characterizing the degree of material gradient in the z- (or ζ-) direction, and the superscript 0 is attached to indicate the z-independent factor in the material coefficient. Again, $\eta = 0$ corresponds to the homogeneous material case.

For transversely isotropic PFGM with the material symmetry axis along the z-axis, the case considered in this paper, the PFGM coefficients in constitutive relations (2.3) and (2.4) can be expressed as

$$[\boldsymbol{C}] = \begin{bmatrix} C_{11}^0 & C_{12}^0 & C_{13}^0 & 0 & 0 & 0 \\ & C_{22}^0 & C_{23}^0 & 0 & 0 & 0 \\ & & C_{33}^0 & 0 & 0 & 0 \\ & & & C_{44}^0 & 0 & 0 \\ & \text{Sym} & & & C_{44}^0 & 0 \\ & & & & & (C_{11}^0 - C_{12}^0)/2 \end{bmatrix} e^{\eta\zeta}, \tag{2.8}$$

$$[\boldsymbol{e}] = \begin{bmatrix} 0 & 0 & 0 & 0 & e_{15}^0 & 0 \\ 0 & 0 & 0 & e_{15}^0 & 0 & 0 \\ e_{31}^0 & e_{31}^0 & e_{33}^0 & 0 & 0 & 0 \end{bmatrix} e^{\eta\zeta}; \quad [\boldsymbol{\varepsilon}] = \begin{bmatrix} \varepsilon_{11}^0 & 0 & 0 \\ 0 & \varepsilon_{11}^0 & 0 \\ 0 & 0 & \varepsilon_{33}^0 \end{bmatrix} e^{\eta\zeta}. \tag{2.9a,b}$$

The derivation of Green's functions will be given in terms of the Cartesian system of vector functions (Pan, 1989a,b):

$$
\begin{aligned}
&L(x, y; \alpha, \beta) = e_z S(x, y; \alpha, \beta), \\
&M(x, y; \alpha, \beta) = (e_x \partial_x + e_y \partial_y) S(x, y; \alpha, \beta), \\
&N(x, y; \alpha, \beta) = (e_x \partial_y - e_y \partial_x) S(x, y; \alpha, \beta)
\end{aligned}
\tag{2.10}
$$

with

$$
S(x, y; \alpha, \beta) = e^{-i(\alpha x + \beta y)}/(2\pi),
\tag{2.11}
$$

where e_x, e_y, and e_z are the unit vectors along the x-, y-, and z- (or ζ-) axes, respectively; α and β are the transformation variables corresponding to the two horizontal physical variables x and y. There are two important features associated with this system of vector functions: (a) To find the plane strain deformation in the (x, z)-plane, one needs only to replace 2π with $\sqrt{2\pi}$ and β with 0, respectively. (b) While the solution in terms of the L and M vectors is contributed to the dilatational deformation, that of the N vector is to the rotational part. Corresponding to the dynamic counterparts, the L and M part is related to the Rayleigh wave while the N part to the Love wave. In this paper we name the solution associated with the L and M vectors as the LM-type solution and that associated with the N vector as N-type solution.

We further add that the scalar function S satisfies the following Helmholtz equation:

$$
\frac{\partial^2 S}{\partial x^2} + \frac{\partial^2 S}{\partial y^2} + \lambda^2 S = 0
\tag{2.12}
$$

with

$$
\lambda = \sqrt{(\alpha^2 + \beta^2)}.
\tag{2.13}
$$

3. General solution and propagator matrix of each layer

In order to derive the general solution for each layer, say layer k, we use the local vertical coordinate ζ instead of the global vertical coordinate z. We first express the elastic displacement, electric potential, traction, electric displacements, body force, and electric charge density in terms of the Cartesian system of vector functions (2.10):

$$
u(x, y, \zeta) = \int \int_{-\infty}^{+\infty} [U_L(\zeta) L(x, y) + U_M(\zeta) M(x, y) + U_N(\zeta) N(x, y)] \, d\alpha \, d\beta,
\tag{3.1}
$$

$$
\phi(x, y, \zeta) = \int \int_{-\infty}^{+\infty} \Phi(\zeta) S(x, y) \, d\alpha \, d\beta,
\tag{3.2}
$$

$$
t(x, y, \zeta) \equiv \sigma_{xz} e_x + \sigma_{yz} e_y + \sigma_{zz} e_z = \int \int_{-\infty}^{+\infty} [T_L(\zeta) L(x, y) + T_M(\zeta) M(x, y) + T_N(\zeta) N(x, y)] \, d\alpha \, d\beta,
\tag{3.3}
$$

$$
D(x, y, \zeta) = \int \int_{-\infty}^{+\infty} [D_L(\zeta) L(x, y) + D_M(\zeta) M(x, y) + D_N(\zeta) N(x, y)] \, d\alpha \, d\beta,
\tag{3.4}
$$

$$
f(x, y, \zeta) = \int \int_{-\infty}^{+\infty} [F_L(\zeta) L(x, y) + F_M(\zeta) M(x, y) + F_N(\zeta) N(x, y)] \, d\alpha \, d\beta,
\tag{3.5}
$$

$$-q(x, y, \zeta) = \int \int_{-\infty}^{+\infty} Q(\zeta) S(x, y) \, \mathrm{d}\alpha \, \mathrm{d}\beta. \tag{3.6}$$

We now take the derivatives of the elastic displacement (3.1) and electric potential (3.2), and substitute the results into the constitutive relations (2.3) and (2.4). The elastic stress and electric displacement can thus be expressed in terms of the Cartesian system of vector functions, as (omitting the integral sign):

$$\sigma_{xx} = \left[C_{11}^0 \left(U_M \frac{\partial^2}{\partial x^2} + U_N \frac{\partial^2}{\partial x \partial y} \right) + C_{12}^0 \left(U_M \frac{\partial^2}{\partial y^2} - U_N \frac{\partial^2}{\partial x \partial y} \right) + C_{13}^0 \frac{\mathrm{d}U_L}{\mathrm{d}\zeta} + e_{31}^0 \frac{\mathrm{d}\varPhi}{\mathrm{d}\zeta} \right] e^{\eta\zeta} S,$$

$$\sigma_{yy} = \left[C_{12}^0 \left(U_M \frac{\partial^2}{\partial x^2} + U_N \frac{\partial^2}{\partial x \partial y} \right) + C_{11}^0 \left(U_M \frac{\partial^2}{\partial y^2} - U_N \frac{\partial^2}{\partial x \partial y} \right) + C_{13}^0 \frac{\mathrm{d}U_L}{\mathrm{d}\zeta} + e_{31}^0 \frac{\mathrm{d}\varPhi}{\mathrm{d}\zeta} \right] e^{\eta\zeta} S,$$

$$\sigma_{zz} = \left[C_{13}^0 U_M \left(\frac{\partial^2}{\partial x^2} + \frac{\partial^2}{\partial y^2} \right) + C_{33}^0 \frac{\mathrm{d}U_L}{\mathrm{d}\zeta} + e_{33}^0 \frac{\mathrm{d}\varPhi}{\mathrm{d}\zeta} \right] e^{\eta\zeta} S,$$

$$\sigma_{yz} = \left[C_{44}^0 \left(U_L \frac{\partial}{\partial y} + \frac{\mathrm{d}U_M}{\mathrm{d}\zeta} \frac{\partial}{\partial y} - \frac{\mathrm{d}U_N}{\mathrm{d}\zeta} \frac{\partial}{\partial x} \right) + e_{15}^0 \varPhi \frac{\partial}{\partial y} \right] e^{\eta\zeta} S, \tag{3.7a–f}$$

$$\sigma_{xz} = \left[C_{44}^0 \left(U_L \frac{\partial}{\partial x} + \frac{\mathrm{d}U_M}{\mathrm{d}\zeta} \frac{\partial}{\partial x} + \frac{\mathrm{d}U_N}{\mathrm{d}\zeta} \frac{\partial}{\partial y} \right) + e_{15}^0 \varPhi \frac{\partial}{\partial x} \right] e^{\eta\zeta} S,$$

$$\sigma_{xy} = C_{66}^0 \left[2 U_M \frac{\partial^2}{\partial x \partial y} + U_N \left(\frac{\partial^2}{\partial y^2} - \frac{\partial^2}{\partial x^2} \right) \right] e^{\eta\zeta} S,$$

$$D_x = \left[e_{15}^0 \left(\frac{\mathrm{d}U_M}{\mathrm{d}\zeta} \frac{\partial}{\partial x} + \frac{\mathrm{d}U_N}{\mathrm{d}\zeta} \frac{\partial}{\partial y} + U_L \frac{\partial}{\partial x} \right) - \varepsilon_{11}^0 \varPhi \frac{\partial}{\partial x} \right] e^{\eta\zeta} S,$$

$$D_y = \left[e_{15}^0 \left(\frac{\mathrm{d}U_M}{\mathrm{d}\zeta} \frac{\partial}{\partial y} - \frac{\mathrm{d}U_N}{\mathrm{d}\zeta} \frac{\partial}{\partial x} + U_L \frac{\partial}{\partial y} \right) - \varepsilon_{11}^0 \varPhi \frac{\partial}{\partial y} \right] e^{\eta\zeta} S, \tag{3.8a–c}$$

$$D_z = \left[e_{31}^0 U_M \left(\frac{\partial^2}{\partial x^2} + \frac{\partial^2}{\partial y^2} \right) + e_{33}^0 \frac{\mathrm{d}U_L}{\mathrm{d}\zeta} - \varepsilon_{33}^0 \frac{\mathrm{d}\varPhi}{\mathrm{d}\zeta} \right] e^{\eta\zeta} S.$$

Comparing (3.7c,d,e) to (3.3), we obtained

$$T_L = \left(-\lambda^2 C_{13}^0 U_M + C_{33}^0 \frac{\mathrm{d}U_L}{\mathrm{d}\zeta} + e_{33}^0 \frac{\mathrm{d}\varPhi}{\mathrm{d}\zeta} \right) e^{\eta\zeta},$$

$$T_M = \left[C_{44}^0 \left(U_L + \frac{\mathrm{d}U_M}{\mathrm{d}\zeta} \right) + e_{15}^0 \varPhi \right] e^{\eta\zeta}, \tag{3.9a–c}$$

$$T_N = C_{44}^0 \frac{\mathrm{d}U_N}{\mathrm{d}\zeta} e^{\eta\zeta}.$$

We now compare the ζ-component of the electric displacement in (3.4) to (3.8c). This gives us

$$D_L = \left(-\lambda^2 e_{31}^0 U_M + e_{33}^0 \frac{\mathrm{d}U_L}{\mathrm{d}\zeta} - \varepsilon_{33}^0 \frac{\mathrm{d}\varPhi}{\mathrm{d}\zeta} \right) e^{\eta\zeta}. \tag{3.10}$$

Substituting Eq. (3.7) into Eq. (2.1), with the body force f being replaced by (3.5), we further found

$$\frac{\mathrm{d}T_L}{\mathrm{d}\zeta} - \lambda^2 T_M + F_L = 0,$$

$$\left(-\lambda^2 C_{11}^0 U_M + C_{13}^0 \frac{\mathrm{d}U_L}{\mathrm{d}\zeta} + e_{31}^0 \frac{\mathrm{d}\varPhi}{\mathrm{d}\zeta} \right) e^{\eta\zeta} + \frac{\mathrm{d}T_M}{\mathrm{d}\zeta} + F_M = 0, \tag{3.11a–c}$$

$$\frac{\mathrm{d}T_N}{\mathrm{d}\zeta} - \lambda^2 C_{66}^0 U_N e^{\eta\zeta} + F_N = 0.$$

Similarly, substitution of (3.4) into (2.2), also making use of (3.6), yields

$$\frac{\mathrm{d}D_L}{\mathrm{d}\zeta} - \lambda^2 e_{15}^0 \left(\frac{\mathrm{d}U_M}{\mathrm{d}\zeta} + U_L\right)e^{\eta\zeta} + \lambda^2 \varepsilon_{11}^0 \Phi e^{\eta\zeta} + Q = 0. \tag{3.12}$$

In (3.11) and (3.12), the expansion coefficients F_L, F_M, F_N, and Q are associated with the body force and electric charge density in the kth layer.

3.1. N-type solution

It is observed from (3.9) to (3.12) that the N-type solution is independent of the rest. This is one of the advantages of using the system of vector functions. Furthermore, the N-type is independent of the electric quantities, i.e., it is purely elastic, with the coefficient equation being

$$[\boldsymbol{E}^N(\zeta)]_{,\zeta} = \begin{bmatrix} 0 & \lambda e^{-\eta\zeta}/C_{44}^0 \\ \lambda e^{\eta\zeta} C_{66}^0 & 0 \end{bmatrix}[\boldsymbol{E}^N(\zeta)] - \begin{bmatrix} 0 \\ F_N/\lambda \end{bmatrix}, \tag{3.13}$$

where

$$[\boldsymbol{E}^N(\zeta)] = [U_N(\zeta), T_N(\zeta)/\lambda]^t. \tag{3.14}$$

An easy and concise way to solve (3.13) is to introduce temporarily the following vector:

$$[\boldsymbol{E}^{N*}(\zeta)] = [U_N(\zeta), T_N(\zeta)e^{-\eta\zeta}/\lambda]^t, \tag{3.15}$$

in terms of which, Eq. (3.13) becomes

$$[\boldsymbol{E}^{N*}]_{,\zeta} = \lambda \begin{bmatrix} 0 & 1/\boldsymbol{C}_{44}^0 \\ \boldsymbol{C}_{66}^0 & -\eta/\lambda \end{bmatrix}[\boldsymbol{E}^{N*}] - \begin{bmatrix} 0 \\ \boldsymbol{F}_N e^{-\eta\zeta}/\lambda \end{bmatrix}. \tag{3.16}$$

The homogeneous solution of (3.16) can be easily found as (Pan, 1989a)

$$[\boldsymbol{E}^{N*}] = [\boldsymbol{Z}^N(\zeta)][\boldsymbol{K}^N], \tag{3.17}$$

where $[\boldsymbol{K}^N]$ is a column coefficient matrix of 2×1 with its elements to be determined by the continuity and/or boundary conditions, and $[\boldsymbol{Z}(\zeta)^N]$ is the solution matrix with elements as

$$[\boldsymbol{Z}^N(\zeta)] = \begin{bmatrix} e^{\lambda s_1 \zeta} & e^{\lambda s_2 \zeta} \\ \bar{s}_1 e^{\lambda s_1 \zeta} & \bar{s}_2 e^{\lambda s_2 \zeta} \end{bmatrix}, \tag{3.18}$$

where

$$s_{1,2} = \frac{-\eta/\lambda \pm \sqrt{(\eta/\lambda)^2 + 4C_{66}^0/C_{44}^0}}{2}; \quad \bar{s}_{1,2} = s_{1,2}C_{44}^0. \tag{3.19a,b}$$

We remark that the two eigenvalues s_1 and s_2 in (3.18) and (3.19) are arranged in such a way so that the real part of s_2 is less than zero.

With the general solution (3.18) for the kth layer, one can derive the corresponding propagating relation, which relates the expansion coefficients U_N and T_N at the upper interface to those at the lower interface of layer k. Using the global vertical coordinates z_{k-1} ($\zeta = 0$) and z_k ($\zeta = h_k$) in (3.17), and evaluating it at the upper and lower interfaces gives

$$[\boldsymbol{E}^N(z_{k-1})] = [\boldsymbol{a}^N(z)][\boldsymbol{E}^N(z_k)], \tag{3.20}$$

where z_{k-1} and z_k are the depths of the upper and lower interfaces of layer k. In (3.20), the propagator matrix $[\boldsymbol{a}]$, also called layer matrix or transfer matrix, is expressed as

$$[\boldsymbol{a}] = [\boldsymbol{B}]\langle e^{-\lambda s_k^* h_k}\rangle [\boldsymbol{B}]^{-1} \begin{bmatrix} 1 & 0 \\ 0 & e^{-\eta_k h_k} \end{bmatrix} \tag{3.21}$$

with

$$\langle e^{-\lambda s_k^* h_k}\rangle = \mathrm{diag}\left[e^{-\lambda s_{k1} h_k}, \quad e^{-\lambda s_{k2} h_k} \right], \tag{3.22}$$

$$[\boldsymbol{B}] = \begin{bmatrix} 1 & 1 \\ \bar{s}_1 & \bar{s}_2 \end{bmatrix}. \tag{3.23}$$

We point out that subscript k is also added to the eigenvalue s, thickness h, and exponential factor η of the layer to indicate that these quantities are associated with layer k.

We further remark that the solution and propagator matrices in terms of the cylindrical system of vector function are exactly the same as (3.18) and (3.21), respectively. Therefore, finding them for one system gives those in the other system. This feature also gives certain numerical advantages when programming these equations.

3.2. LM-type solution

For this type of deformation, the elastic and piezoelectric fields are coupled together, and from equations (3.9) to (3.12), a compact form of the equation can be recast into

$$[U_L, U_M, T_L, T_M, \Phi, D_L]^t_{,\zeta} = [\boldsymbol{A}][U_L, U_M, T_L, T_M, \Phi, D_L]^t + [0, 0, -F_L, -F_M, 0, -Q]^t, \tag{3.24}$$

where the nonzero elements of the 6×6 matrix $[\boldsymbol{A}]$ is given in Appendix B. It is remarked that all the diagonal elements of $[\boldsymbol{A}]$ are zero, a feature that will be used soon.

We now temporarily introduce the following vector:

$$[\boldsymbol{E}^*] = [U_L, \lambda U_M, T_L e^{-\eta\zeta}/\lambda, T_M e^{-\eta\zeta}, \Phi, D_L e^{-\eta\zeta}/\lambda]^t. \tag{3.25}$$

Then (3.24) becomes

$$[\boldsymbol{E}^*]_{,\zeta} = \lambda[\boldsymbol{W}][\boldsymbol{E}^*] + [\boldsymbol{F}], \tag{3.26}$$

where the force expansion column vector is

$$[\boldsymbol{F}] = [0, 0, -F_L e^{-\eta\zeta}/\lambda, -F_M e^{-\eta\zeta}, 0, -Q e^{-\eta\zeta}/\lambda]^t. \tag{3.27}$$

The nonzero elements of the 6×6 matrix $[\boldsymbol{W}]$ in (3.26) is given in Appendix C. It is noticed that matrix $[\boldsymbol{W}]$ is independent of the vertical coordinate z or ζ, but is a function of parameters η and λ.

In order to find the homogeneous solution of (3.26), we assume that

$$[\boldsymbol{E}^*(\zeta)] = [\boldsymbol{b}]e^{\lambda v\zeta}. \tag{3.28}$$

Substituting (3.28) into (3.26) and noticing that all the diagonal elements of $[\boldsymbol{W}]$ are zero gives the following 6-dimension eigenequations for the corresponding homogeneous part of (3.26)

$$\{[\boldsymbol{W}] - v[\boldsymbol{I}]\}[\boldsymbol{b}] = 0, \tag{3.29}$$

where $[\boldsymbol{I}]$ is the 6×6 identity matrix.

We point out again that the eigenvalues and their corresponding eigenvectors of (3.28) depend on the integral variable λ and the FGM exponential factor η. Therefore, these eigenequations need to be solved for different η and for each integration point λ.

Assuming that the 6 eigenvalues v_i are distinct, the general solution corresponding to the homogeneous part of (3.26) is found to be

$$[E^*(\zeta)] = [Z(\zeta)][K], \tag{3.30}$$

where $[K]$ is a 6×1 coefficient matrix with its elements to be determined by the interface and/or boundary conditions, and

$$[Z(\zeta)] = [B]\langle e^{\lambda v * \zeta}\rangle \tag{3.31}$$

with

$$\langle e^{\lambda v * \zeta}\rangle = \mathrm{diag}\left[e^{\lambda v_1 \zeta}, e^{\lambda v_2 \zeta}, e^{\lambda v_3 \zeta}, e^{\lambda v_4 \zeta}, e^{\lambda v_5 \zeta}, e^{\lambda v_6 \zeta}\right], \tag{3.32}$$

$$[B] = [b_1, b_2, b_3, b_4, b_5, b_6]. \tag{3.33}$$

It is noted that the real parts of the first three eigenvalues are positive and those of the remaining three are negative.

In order to use the propagating relation for the multilayered structure, we introduce the following set of coefficients:

$$[E] = [U_L, \lambda U_M, T_L/\lambda, T_M, \Phi, D_L/\lambda]^t, \tag{3.34}$$

which is related to $[E^*]$ as

$$[E] = \langle P\rangle[E^*], \tag{3.35}$$

where $\langle P\rangle$ is a 6×6 diagonal matrix defined as

$$\langle P\rangle = \mathrm{diag}\left[1, 1, e^{\eta \zeta}, e^{\eta \zeta}, 1, e^{\eta \zeta}\right]. \tag{3.36}$$

The propagating relation in terms of the coefficient vector $[E]$ of kth layer, which connects the values at the global coordinate z_{k-1} ($\zeta = 0$) to those at z_k ($\zeta = h_k$), is found to be

$$[E(z_{k-1})] = [a][E(z_k)], \tag{3.37}$$

where

$$[a] = [B]\langle e^{-\lambda v * h_k}\rangle[B]^{-1}\langle Q\rangle \tag{3.38}$$

is the propagator matrix for the LM-type deformation, and

$$\langle e^{-\lambda v * h_k}\rangle = \mathrm{diag}\left[e^{-\lambda v_1 h_k}, e^{-\lambda v_2 h_k}, e^{-\lambda v_3 h_k}, e^{-\lambda v_4 h_k}, e^{-\lambda v_5 h_k}, e^{-\lambda v_6 h_k}\right], \tag{3.39}$$

$$\langle Q\rangle = \mathrm{diag}\left[1, 1, e^{-\eta_k h_k}, e^{-\eta_k h_k}, 1, e^{-\eta_k h_k}\right]. \tag{3.40}$$

Similar to the N-type solution, the solution and propagator matrices in terms of the cylindrical system of vector functions are exactly the same as those given by (3.31) and (3.38). We emphasize again that this feature possesses certain numerical advantages when programming these equations. It is further noted that in solving the eigenequation (3.29), we have assumed that all the eigenvalues are distinct. Should repeated eigenvalues occur, a slight perturbation on the material properties can be used to make all the eigenvalues distinct with neglected errors so that the solution developed in this paper can still be directly used.

4. Source function in transformed domain

In order to derive Green's functions in the layered system, we also need to specify the point source. We assume, without loss of generality, that in the kth layer, there is a point-force/point-charge density located

along the z-axis at the depth $z = d$ or locally at $\zeta = h_{k1}$ (Fig. 1). Therefore, in terms of the local vertical coordinate ζ, along with the two horizontal coordinates, the point force and point charge density can be expressed as

$$f_i(x, y, \zeta) = \delta(x)\delta(y)\delta(\zeta - h_{k1})n_i, \tag{4.1}$$

$$-q(x, y, \zeta) = \delta(x)\delta(y)\delta(\zeta - h_{k1}), \tag{4.2}$$

where n_i is the direction cosines of the point force. Expanding these expressions using (3.5) and (3.6), we found the expansion coefficients as (Pan, 1999)

$$\begin{aligned}
F_L &= \frac{n_z}{2\pi}\delta(\zeta - h_{k1}), \\
F_M &= \frac{n_x\alpha + n_y\beta}{2\pi\lambda^2}\delta(\zeta - h_{k1}), \\
F_N &= \frac{n_x\beta - n_y\alpha}{2\pi\lambda^2}\delta(\zeta - h_{k1}),
\end{aligned} \tag{4.3}$$

$$Q = \frac{-1}{2\pi}\delta(\zeta - h_{k1}). \tag{4.4}$$

The expansion coefficients for the corresponding 2D plane strain deformation can be obtained from (4.3) and (4.4) by replacing 2π with $\sqrt{2\pi}$ and β with 0, respectively.

The concentrated force and electric charge density will induce discontinuities in the expansion coefficients of the traction and normal electric displacement component, which are found to be

$$\Delta T_L \equiv T_L(h_{k1} + 0) - T_L(h_{k1} - 0) = \frac{-n_z}{2\pi},$$

$$\Delta T_M \equiv T_M(h_{k1} + 0) - T_M(h_{k1} - 0) = -\frac{n_x\alpha + n_y\beta}{2\pi\lambda^2}, \tag{4.5}$$

$$\Delta T_N \equiv T_N(h_{k1} + 0) - T_N(h_{k1} - 0) = -\frac{n_x\beta - n_y\alpha}{2\pi\lambda^2},$$

$$\Delta D_L \equiv D_L(h_{k1} + 0) - D_L(h_{k1} - 0) = \frac{1}{2\pi}. \tag{4.6}$$

5. Green's functions in transformed domain

For a source situated at depth $z = d$ in layer k, we divide the source layer into two sub-layers, $k1$ and $k2$, with identical properties. Because of the source, some of the components in functions $[\boldsymbol{E}(z)]$ and $[\boldsymbol{E}^N(z)]$ are discontinuous across $z = d$, as we have obtained in the previous section. In general, the discontinuities can be defined as

$$\begin{aligned}
[\Delta\boldsymbol{E}] &\equiv [\boldsymbol{E}_{k2}(d)] - [\boldsymbol{E}_{k1}(d)], \\
[\Delta\boldsymbol{E}^N] &\equiv [\boldsymbol{E}_{k2}^N(d)] - [\boldsymbol{E}_{k1}^N(d)],
\end{aligned} \tag{5.1a,b}$$

with their discontinuity components being given by (4.5) and (4.6).

Propagating the solutions from $z = d - 0$, which is just above the source, to the surface $z = 0$, we obtain

$$[\boldsymbol{E}(0)] = [\boldsymbol{a}_1][\boldsymbol{a}_2]\cdots[\boldsymbol{a}_{k1}][\boldsymbol{E}_{k1}(d)],$$
$$[\boldsymbol{E}^N(0)] = [\boldsymbol{a}_1^N][\boldsymbol{a}_2^N]\cdots[\boldsymbol{a}_{k1}^N][\boldsymbol{E}_{k1}^N(d)]. \tag{5.2a,b}$$

Similarly, propagating the solutions from the half space $z = H$ to $z = d + 0$, which is just below the source, we have

$$[\boldsymbol{E}_{k2}(h)] = [\boldsymbol{a}_{k2}][\boldsymbol{a}_{k+1}]\cdots[\boldsymbol{a}_p][\boldsymbol{Z}_p(H)][\boldsymbol{K}_p],$$
$$[\boldsymbol{E}_{k2}^N(h)] = [\boldsymbol{a}_{k2}^N][\boldsymbol{a}_{k+1}^N]\cdots[\boldsymbol{a}_p^N][\boldsymbol{Z}_p^N(H)][\boldsymbol{K}_p^N] \tag{5.3a,b}$$

with the undetermined coefficients having the structure as

$$[\boldsymbol{K}_p] = [0, 0, 0, *, *, *]^t,$$
$$[\boldsymbol{K}_p^N] = [0, *]^t, \tag{5.4a,b}$$

where the symbol '*' represents coefficient to be determined. The structure of (5.4) is chosen to satisfy the requirement that the solution vanishes when z approaches $+\infty$. From (5.1), (5.2) and (5.3), we find

$$[\boldsymbol{E}(0)] = [\boldsymbol{G}][\boldsymbol{K}_p] - [\boldsymbol{R}],$$
$$[\boldsymbol{E}^N(0)] = [\boldsymbol{G}^N][\boldsymbol{K}_p^N] - [\boldsymbol{R}^N], \tag{5.5a,b}$$

where

$$[\boldsymbol{G}] = [\boldsymbol{a}_1][\boldsymbol{a}_2]\cdots[\boldsymbol{a}_p][\boldsymbol{Z}_p(H)],$$
$$[\boldsymbol{G}^N] = [\boldsymbol{a}_1^N][\boldsymbol{a}_2^N]\cdots[\boldsymbol{a}_p^N][\boldsymbol{Z}_p^N(H)],$$
$$[\boldsymbol{R}] = [\boldsymbol{a}_1][\boldsymbol{a}_2]\cdots[\boldsymbol{a}_{k-1}][\boldsymbol{a}_{k1}][\Delta\boldsymbol{E}],$$
$$[\boldsymbol{R}^N] = [\boldsymbol{a}_1^N][\boldsymbol{a}_2^N]\cdots[\boldsymbol{a}_{k-1}^N][\boldsymbol{a}_{k1}^N][\Delta\boldsymbol{E}^N]. \tag{5.6a–d}$$

Using the boundary conditions at $z = 0$, the unknown coefficients in $[\boldsymbol{K}_p]$ and $[\boldsymbol{K}_p^N]$ can be determined. As an example, we assume that the boundary condition at the surface of the layered half space is traction-free insulating or traction-free conducting. Then the corresponding constraints for the expansion coefficients are, respectively,

$$T_L(0) = T_M(0) = T_N(0) = D_L(0) = 0,$$
$$T_L(0) = T_M(0) = T_N(0) = \Phi(0) = 0. \tag{5.7a,b}$$

In either case, we have four conditions to determine the four unknowns in $[\boldsymbol{K}_p]$ and $[\boldsymbol{K}_p^N]$. After the unknown coefficients in $[\boldsymbol{K}_p]$ and $[\boldsymbol{K}_p^N]$ are determined, the expansion coefficients at any depth (e.g., for $z \geqslant d$ in layer k, i.e., $z_{k-1} \leqslant z \leqslant z_k$) can be obtained exactly as

$$[\boldsymbol{E}(z)] = [\boldsymbol{a}_{k2}(z - z_{k-1})][\boldsymbol{a}_{k+1}]\cdots[\boldsymbol{a}_p][\boldsymbol{Z}_p(H)][\boldsymbol{K}_p],$$
$$[\boldsymbol{E}^N(z)] = [\boldsymbol{a}_{k2}^N(z - z_{k-1})][\boldsymbol{a}_{k+1}^N]\cdots[\boldsymbol{a}_p^N][\boldsymbol{Z}_p^N(H)][\boldsymbol{K}_p^N]. \tag{5.8a,b}$$

As discussed in Pan (1997) and Yue and Yin (1998), overflow may occur from multiplication of matrices in Eqs. (5.6) and (5.8). This can be overcome by factoring out the exponentially growing factor in the elements of the propagator matrix and propagating the matrix either forward or backward, depending on the relative location of the source and field points. Since in the modified propagator matrices, no element is exponentially growing, there will be no overflow problem for a multilayered half space having any number of layers with any thickness for each layer.

6. Physical-domain solutions

Green's functions obtained above in the transformed domain need to be integrated numerically to find the physical-domain solutions. Since in terms of the cylindrical system of vector functions, the individual components of Green's functions will be in the cylindrical coordinates. We found that, in order to find all the elastic and electric quantities (elastic displacements, strains, and stresses; electric potential, electric fields, and electric displacements) due to three point forces and a negative point charge density, only 38 integrals need to be evaluated.

It is further noted that the integrands in the infinite integrals for Green's functions involve Bessel functions that are oscillatory and go to zero slowly when their variable approaches infinity. Thus, the common numerical integral methods, such as the trapezoidal rule or Simpson's rule, are not suitable for such integrations. On the other hand, numerical integration of this type of functions via the adaptive Gauss quadrature (Chave, 1983; Lucas, 1995) has been found to be very accurate and efficient. We therefore have adopted and modified this algorithm to the evaluation of Green's functions in the PFGM multilayered half space.

Let us express the infinite integral for each Green's function as a summation of partial integration terms:

$$\int_0^{+\infty} f(\lambda, z) J_m(\lambda r) \, d\lambda = \sum_{n=1}^{N} \int_{\lambda_n}^{\lambda_{n+1}} f(\lambda, z) J_m(\lambda r) \, d\lambda. \tag{6.1}$$

In each subinterval, a starting 3-point Gauss rule is applied to approximate the integral. A combined relative-absolute error criterion is used to check the results. If the error criterion is not satisfied, new Gauss points are added optimally so that only the new integrand values need to be calculated. This procedure continues until the selected error criterion is satisfied (Chave, 1983; Lucas, 1995). In the numerical analysis presented below, we have set the relative and absolute errors, respectively, at 10^{-3} and 10^{-4}.

Another important issue on the PFGM Green's functions we should remark is their singularity behavior, and this is required in future implementation of these Green's functions into any BEM program for PFGMs. Although the expression for the total PFGM Green's function near the singular (source) point could be very complicated even for a single PFGM space, the singular part near the source point turns out to be exactly the same as that in the corresponding no-PFGM space. In other words, Green's function for a single PFGM space can be always expressed as a summation of two parties near the singular point, just as for the corresponding 3D and 2D elastic FGM space (Martin et al., 2002; Chan et al., 2004):

$$\boldsymbol{G}(\boldsymbol{x}; \boldsymbol{x}') = e^{-\boldsymbol{\eta} \cdot (\boldsymbol{x} + \boldsymbol{x}')} [\boldsymbol{G}^0(\boldsymbol{x}; \boldsymbol{x}') + \boldsymbol{G}^g(\boldsymbol{x}; \boldsymbol{x}')], \tag{6.2}$$

where $\boldsymbol{\eta} = \eta \boldsymbol{e}_z$, $\boldsymbol{x}$ and $\boldsymbol{x}'$ are, respectively, the field and source point, $\boldsymbol{G}^0$ Green's function corresponding to the no FGM space, and $\boldsymbol{G}^g$ the additional grading term, which is a bounded and well-behaved function of the distance between the field and source points. Since the grading term $\boldsymbol{G}^g$ is bounded as $|\boldsymbol{x} - \boldsymbol{x}'| \to 0$, the singularity is only contained within $\boldsymbol{G}^0$. Therefore, in the numerical calculation of the PFGM Green's functions, the subtraction-addition approach that we proposed for the layered system (Pan et al., 2001) can be utilized to handle the singularity issue easily, no matter if the system is layered, FGM, or layered PFGM.

The original program was written for one Hankel transform only. In our case, evaluation of 38 infinite integrals is required in order to obtain all the elastic and electric components. Thus, direct application of the original adaptive Gauss quadrature would result in intensive computation because of the multiplication of the propagator matrices involved. However, we noticed that the integrand $f(\lambda, z)$ in (6.1), which represents one of the expansion coefficients in (5.8), is actually the result of the multiplication of the propagator matrices. Since for a given layered half space, the propagator matrix depends only upon the integral variable λ, the original program can therefore be modified in such a way that for all the elastic and electric components, the multiplication of the propagator matrices needs to be evaluated only once for a given Gauss

quadrature point λ. Such a modification to the original adaptive Gauss quadrature saves substantial computation time when calculating all Green's components (Pan, 1997).

7. Numerical results and discussion

Before applying our Green's functions to the multilayered PFGM system, we first checked the reduced purely elastic and piezoelectric layered cases (i.e., the exponential factor $\eta = 0$). We found that the results from the present multilayered PFGM Green's functions are exactly the same as those from previous solutions (Pan, 1997, 2002; Pan and Han, 2004).

In our numerical studies, the layered PFGM half space is made of two transversely isotropic piezoelectric materials: One is the poled lead–zirconate–titanate (PZT-4) ceramic, the other is BaTiO$_3$, with their properties given in Appendix D. Two different models are studied in this paper. The first model is a PFGM half space made of PZT-4 (Fig. 2). The PFGM half space is under a point force (1 N) on the surface, and the response is calculated in the vertical plane ($y = 0$) for x and z varying from 0 to 0.3 m. The second model is a homogeneous half space made of BaTiO$_3$, coated with a PFGM layer of thickness 0.1 m and made of PZT-4. The point source is at (0, 0, 0.15 m), and the response is calculated along a surface line from (0, 0, 0) to (0.3 m, 0, 0) and a vertical line from (0.1 m, 0, 0) to (0.1 m, 0, 0.3 m). For both models, the traction-free insulating boundary condition is assumed at the surface of the layered half space.

We also point out that all the numerical results presented below are dimensionless. Thus, by multiplying L (=1 m), we change the coordinate into the dimensional one. In order to obtain the dimensional elastic displacement, electric potential, stress, and electric displacement (e.g. for stress in N/m^2 and electric displacement in C/m^2), one needs to carry out the following simple multiplication or division (with $C_{max}^0 = 1.66 \times 10^{11}$ N/m^2 and $e_{max}^0 = 18.6$ C/m^2):

 (i) for the elastic displacement due to a point force, divide the result by $C_{max}^0 L$;
 (ii) for the elastic displacement due to a negative point charge density or the electric potential due to a point force, divide the result by $e_{max}^0 L$;
(iii) for the electric potential due to a negative point charge density, multiply the result by $C_{max}^0/(e_{max}^0 e_{max}^0 L)$;
(iv) for the stress due to a point force or the electric displacement due to a negative point charge density, divide the result by L^2;
 (v) for the stress due to a negative point charge density, multiply the result by $C_{max}^0/(e_{max}^0 L^2)$;
(vi) for the electric displacement due to a point force, multiply the result by $e_{max}^0/(C_{max}^0 L^2)$.
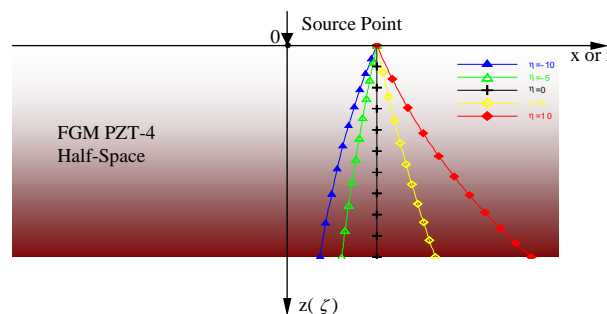

Fig. 2. Geometry of the PFGM PZT-4 half space. The variation of the proportional factor $e^{\eta z}$ in the PFGM half space is shown for $\eta = -10, -5, 0, 5, 10$.
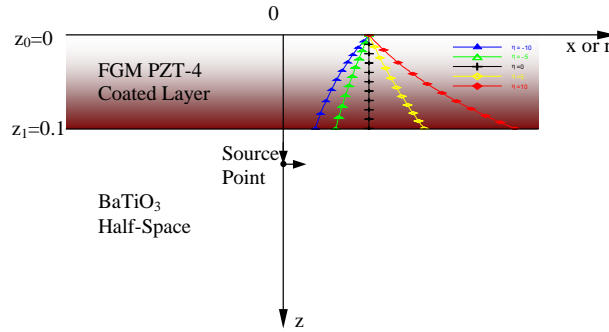
Fig. 3. Geometry of a coated PFGM layer of PZT-4 over a homogeneous half space of BaTiO$_3$. The variation of the proportional factor $e^{\eta z}$ in the coated PFGM layer of PZT-4 is shown for $\eta = -10, -5, 0, 5, 10$.

7.1. Response in the PFGM half space

This corresponds to the first model, which is a PFGM half space made of PZT-4 (Fig. 2). Figs. 4–8 show, respectively, contours of the horizontal elastic displacement u_x, electric potential ϕ horizontal and vertical stress components σ_{xx} and σ_{zz}, and vertical electric displacement D_z in the $y = 0$ plane due to a vertical point force of magnitude 1 N applied at the origin. For each physical quantity, five figures are presented (e.g., Figs. 4a–e) which correspond to the five exponential factors $\eta = -10, -5, 0, 5$, and 10. While a negative exponential factor corresponds to a stiff surface, a positive factor to a soft surface. It can be clearly observed from these figures that for different exponential factors η, the contour shapes and the magnitudes of the physical quantity are completely different. Furthermore, either a stiff (Figs. 4a,b, 5a,b for $\eta = -10$, -5) or a soft (Figs. 4d,e, 5d,e for $\eta = 5, 10$) surface of the PFGM half space will, in general, correspond to a relatively large magnitude in the horizontal elastic displacement u_x and electric potential ϕ, as compared to the corresponding homogeneous half space ($\eta = 0$). On the other hand, the magnitude of the stresses and electric displacements increases with increasing exponential factor η. In other words, the magnitudes of these Green's components are smaller in a PFGM half space with a stiff surface (Figs. 6a,b, 7a,b, 8a,b for $\eta = -10$, -5) than those in the corresponding PFGM half space with a soft surface (Figs. 6d,e, 7d,e, 8d,e for $\eta = 5, 10$).

7.2. Response in the PFGM coated half space

This corresponds to the second model in which the homogeneous half space is made of BaTiO$_3$, coated on its top is a PFGM layer of thickness 0.1 m made of PZT-4 (Fig. 3). In the numerical examples studied in this section, the source point is located along the z-axis in the homogeneous half space with coordinates (0.0, 0.0, 0.15 m) (Fig. 3). The point force has a magnitude of 1 N and negative point charge density has a magnitude of 1 C.

7.2.1. Surface response in the PFGM coated half space

Figs. 9a–c show, respectively, the horizontal elastic displacement u_x, electric potential ϕ, and horizontal electric displacement D_x along a surface line (from (0, 0, 0) to (0.3 m, 0, 0)) of the PFGM half space caused by the vertical point force of 1 N at (0.0, 0.0, 0.15 m). It is observed from Figs. 9b and c that the magnitude of the electric components (i.e., the electric potential ϕ and horizontal electric displacement D_x) decreases with increasing exponential factor η. For the horizontal elastic displacement u_x, however, the same trend follows only for the exponential factor η less or equal to zero (Fig. 9a). For $\eta > 0$, the magnitude of u_x increases with increasing exponential factor η (Fig. 9a).
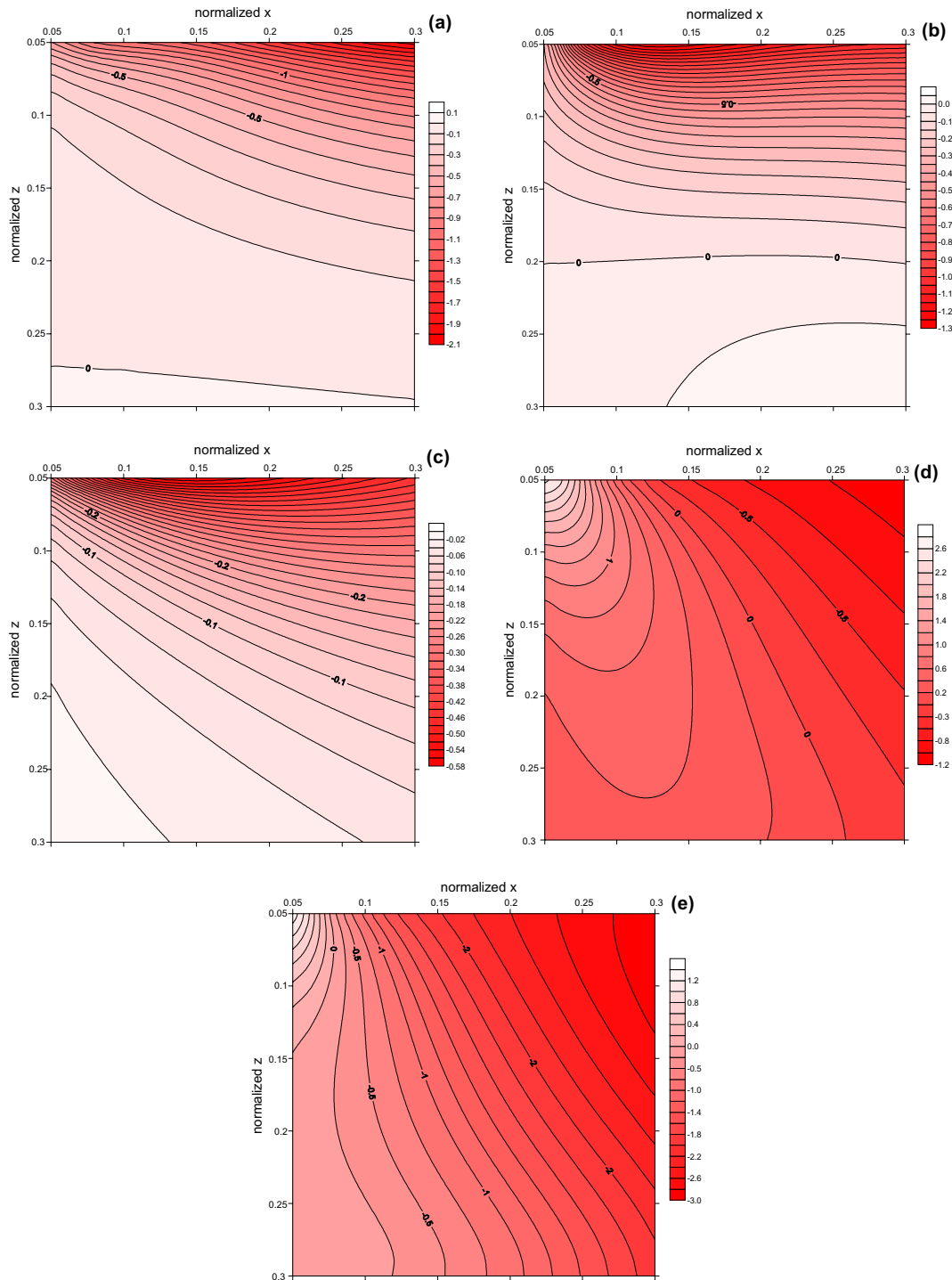
Fig. 4. Contours of the elastic displacement component u_x in the $y = 0$ plane of the PFGM PZT-4 half space due to a vertical point force F_z of magnitude 1 N applied on the surface at the origin (0, 0, 0). To avoid singularity at the origin, x and z are chosen to vary from 0.05 m to 0.3 m. (a)–(e) show, respectively, the contours of u_x for the exponential factors $\eta = -10, -5, 0, 5,$ and 10.
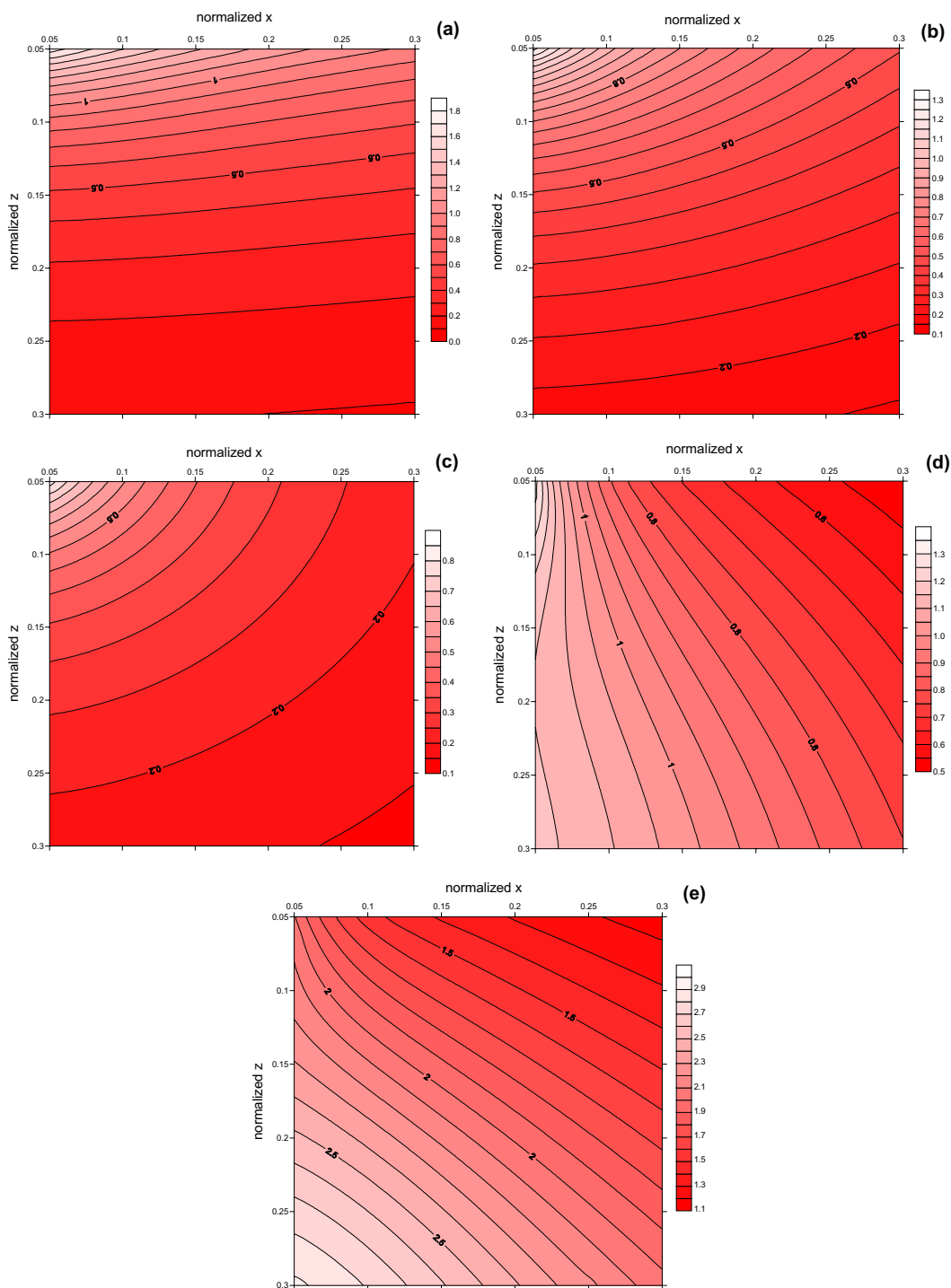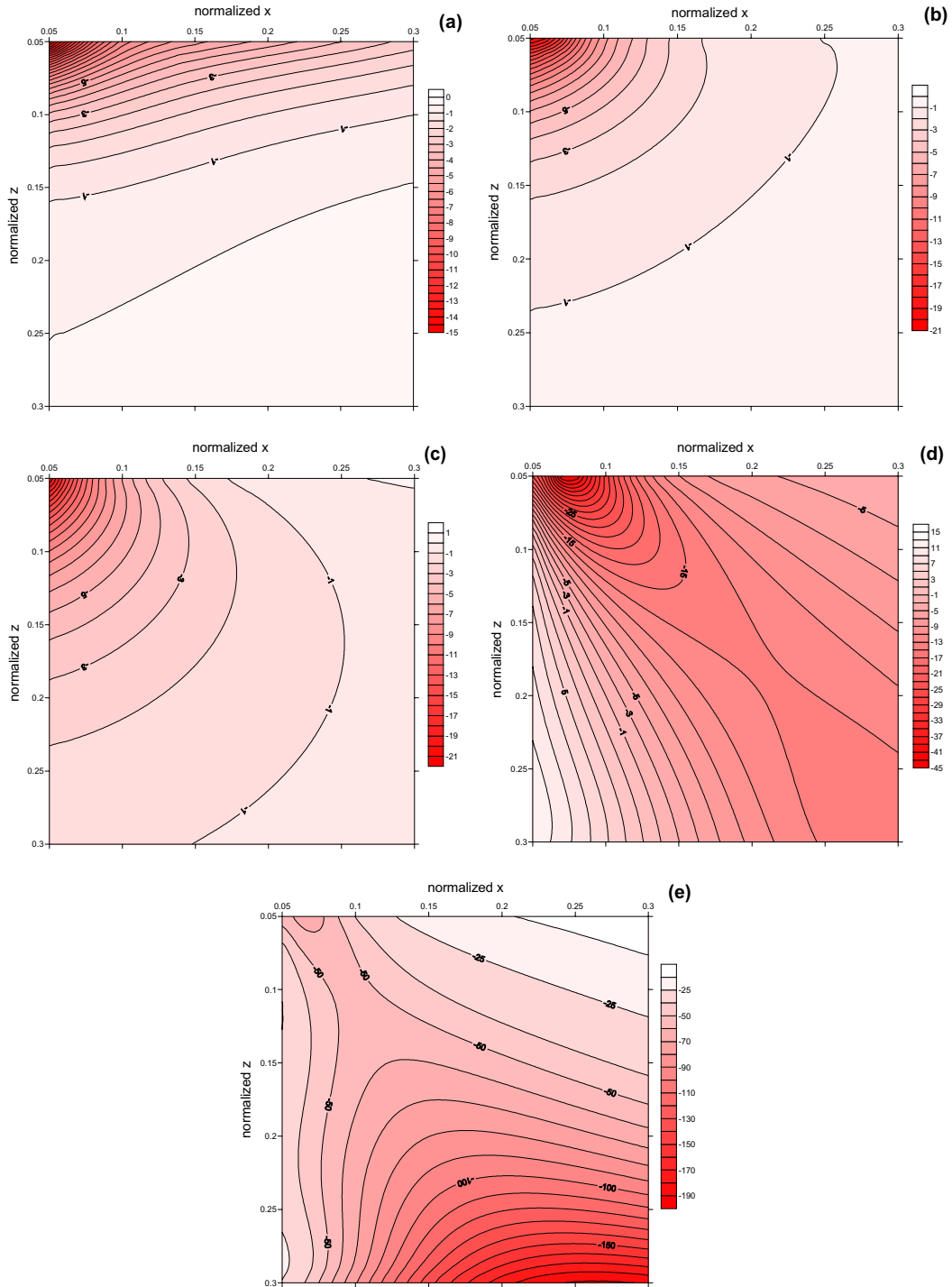
Fig. 5. Contours of the electric potential ϕ in the $y = 0$ plane of the PFGM PZT-4 half space due to a vertical point force F_z of magnitude 1 N applied on the surface at the origin $(0, 0, 0)$. To avoid singularity at the origin, x and z are chosen to vary from 0.05 m to 0.3 m. (a)–(e) show, respectively, the contours of ϕ for the exponential factors $\eta = -10, -5, 0, 5,$ and 10.
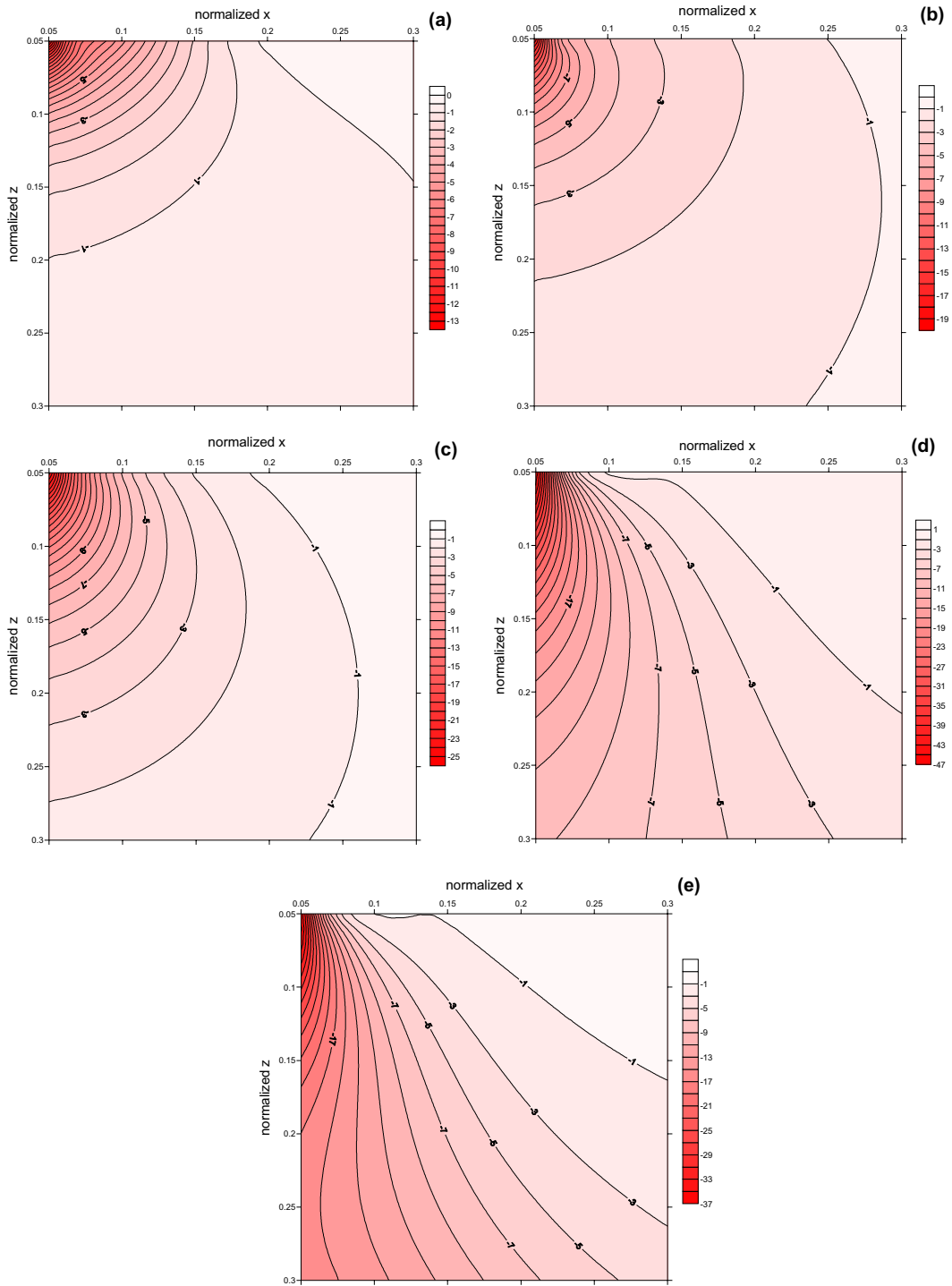
Fig. 6. Contours of the stress component σ_{xx} in the $y = 0$ plane of the PFGM PZT-4 half space due to a vertical point force F_z of magnitude 1 N applied on the surface at the origin (0, 0, 0). To avoid singularity at the origin, x and z are chosen to vary from 0.05 m to 0.3 m. (a)–(e) show, respectively, the contours of σ_{xx} for the exponential factors $\eta = -10$, -5, 0, 5, and 10.
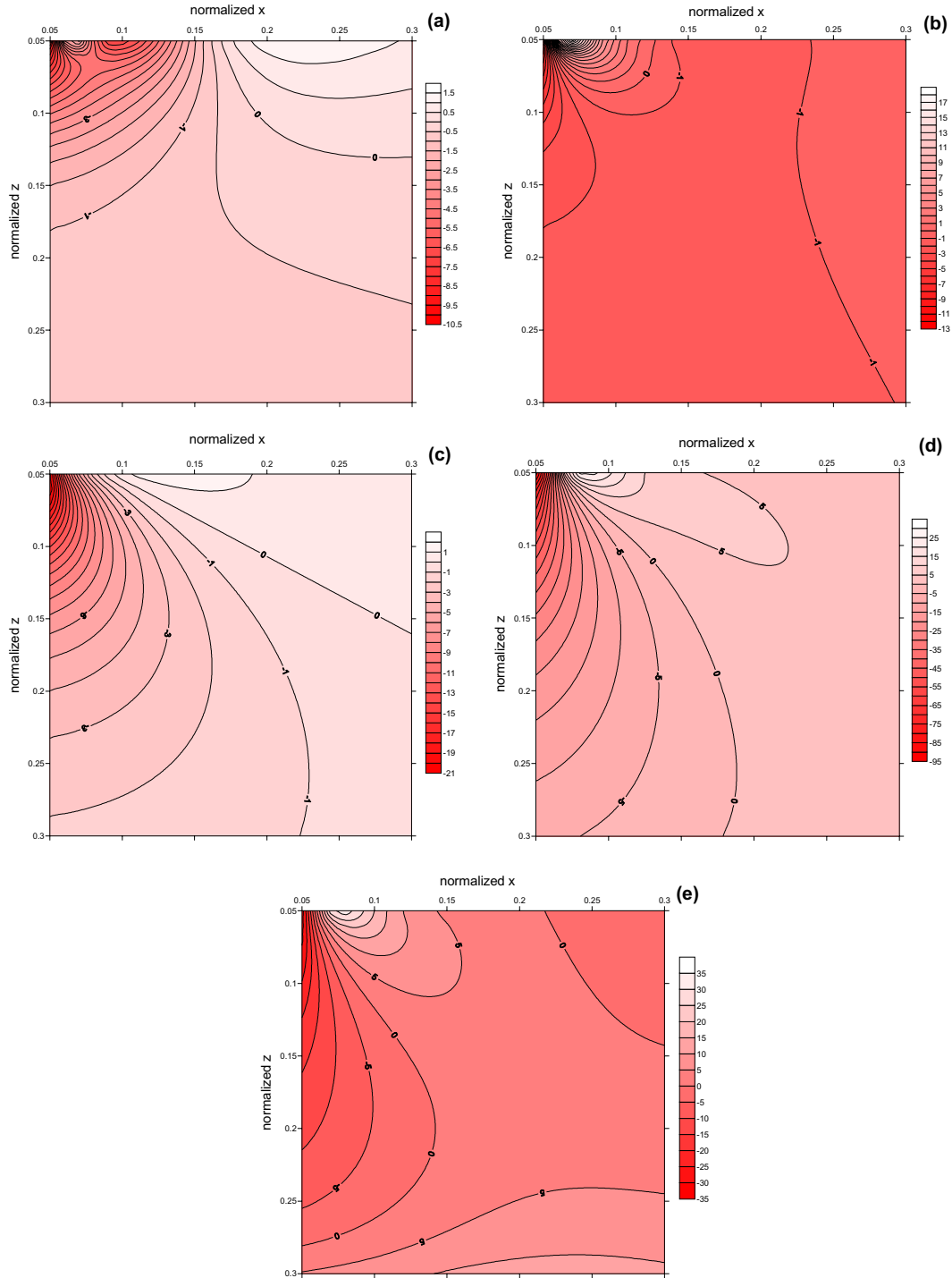
Fig. 7. Contours of the stress component σ_{zz} in the $y = 0$ plane of the PFGM PZT-4 half space due to a vertical point force F_z of magnitude 1 N applied on the surface at the origin $(0, 0, 0)$. To avoid singularity at the origin, x and z are chosen to vary from 0.05 m to 0.3 m. (a)–(e) show, respectively, the contours of σ_{zz} for the exponential factors $\eta = -10$, -5, 0, 5, and 10.

Fig. 8. Contours of the electric displacement component D_z in the $y = 0$ plane of the PFGM PZT-4 half space due to a vertical point force F_z of magnitude 1 N applied on the surface at the origin $(0, 0, 0)$. To avoid singularity at the origin, x and z are chosen to vary from 0.05 m to 0.3 m. (a)–(e) show, respectively, the contours of D_z for the exponential factors $\eta = -10$, -5, 0, 5, and 10.
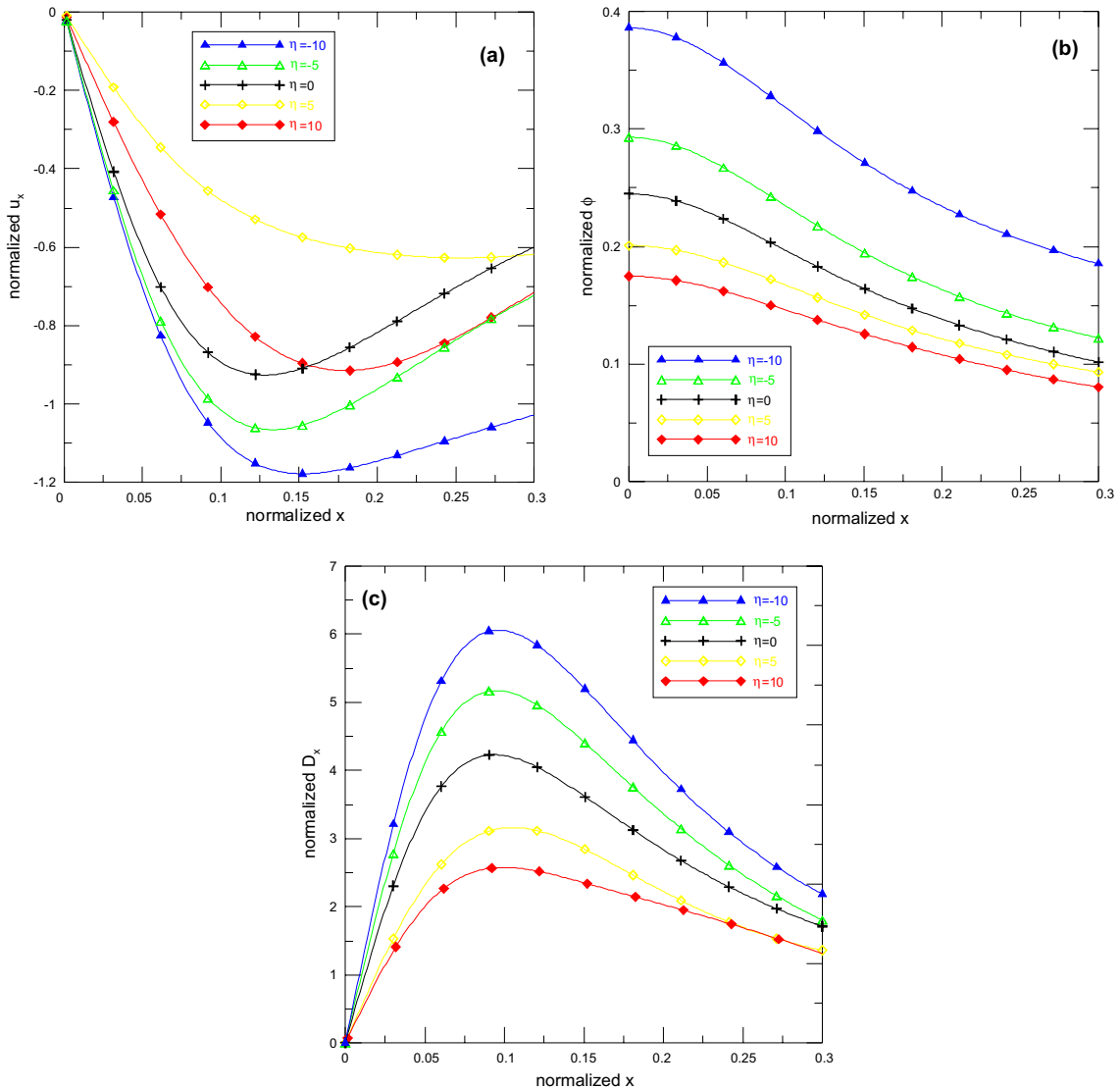
Fig. 9. Variation of the field quantities along a line on the surface (from $(0, 0, 0)$ to $(0.3 \, \text{m}, 0, 0)$) of the PFGM coated half space for the exponential factors $\eta = -10$, -5, 0, 5, and 10, due to a vertical point force F_z of magnitude 1 N applied at $(0, 0, 0.15 \, \text{m})$. Elastic displacement component u_x in (a), electric potential ϕ in (b), and electric displacement component D_x in (c).

7.2.2. Internal response in the PFGM coated half space

Figs. 10a–d show, respectively, the vertical elastic displacement u_z, horizontal stress component σ_{xx}, electric potential ϕ, and horizontal electric displacement D_x along the vertical line (from $(0.1 \, \text{m}, 0, 0)$ to $(0.1 \, \text{m}, 0, 0.3 \, \text{m})$) due to the horizontal point force of 1 N at $(0.0, 0.0, 0.15 \, \text{m})$. First of all, different exponential factors η can have a pronounced influence on the responses in the PFGM layer. Second, it is noted that even though the half space is a homogeneous material made of $BaTiO_3$, the exponential factor η within the PFGM coated layer can still effect the responses within the homogeneous half space, in
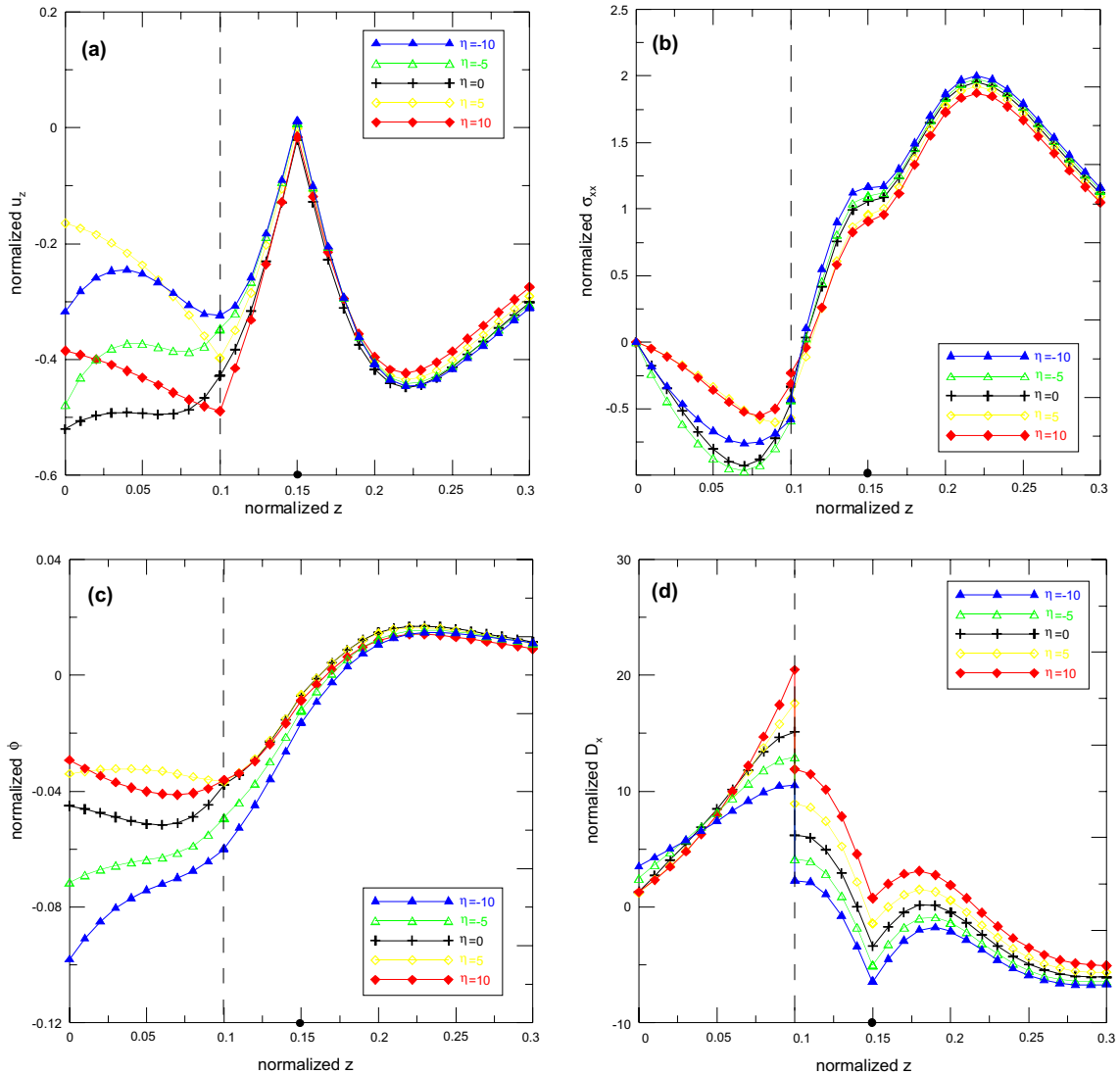
Fig. 10. Variation of the field quantities along a vertical line (from (0.1 m, 0, 0) to (0.1 m, 0, 0.3 m)) of the PFGM coated half space for the exponential factors $\eta = -10, -5, 0, 5,$ and 10, due to a horizontal point force F_x of magnitude 1 N applied at (0, 0, 0.15 m). Elastic displacement component u_z in (a), stress component σ_{xx} in (b), electric potential ϕ in (c), and electric displacement component D_x in (d).

particular in the region close to the interface between the PFGM layer and the homogeneous half space (Figs. 10a–d). More specifically, compared the horizontal electric displacement D_x (Fig. 10d) with the horizontal stress component σ_{xx} (Fig. 10b), we observe that the electric displacement is more sensitive to the exponential factor η than the stress does. Finally, it is further noticed that across the source level at $z = 0.15$ m, while the slopes of the vertical elastic displacement u_z and horizontal electric displacement D_x are discontinuous (Figs. 10a and d), those of the horizontal stress component σ_{xx} and electric potential ϕ are continuous (Figs. 10b and c).
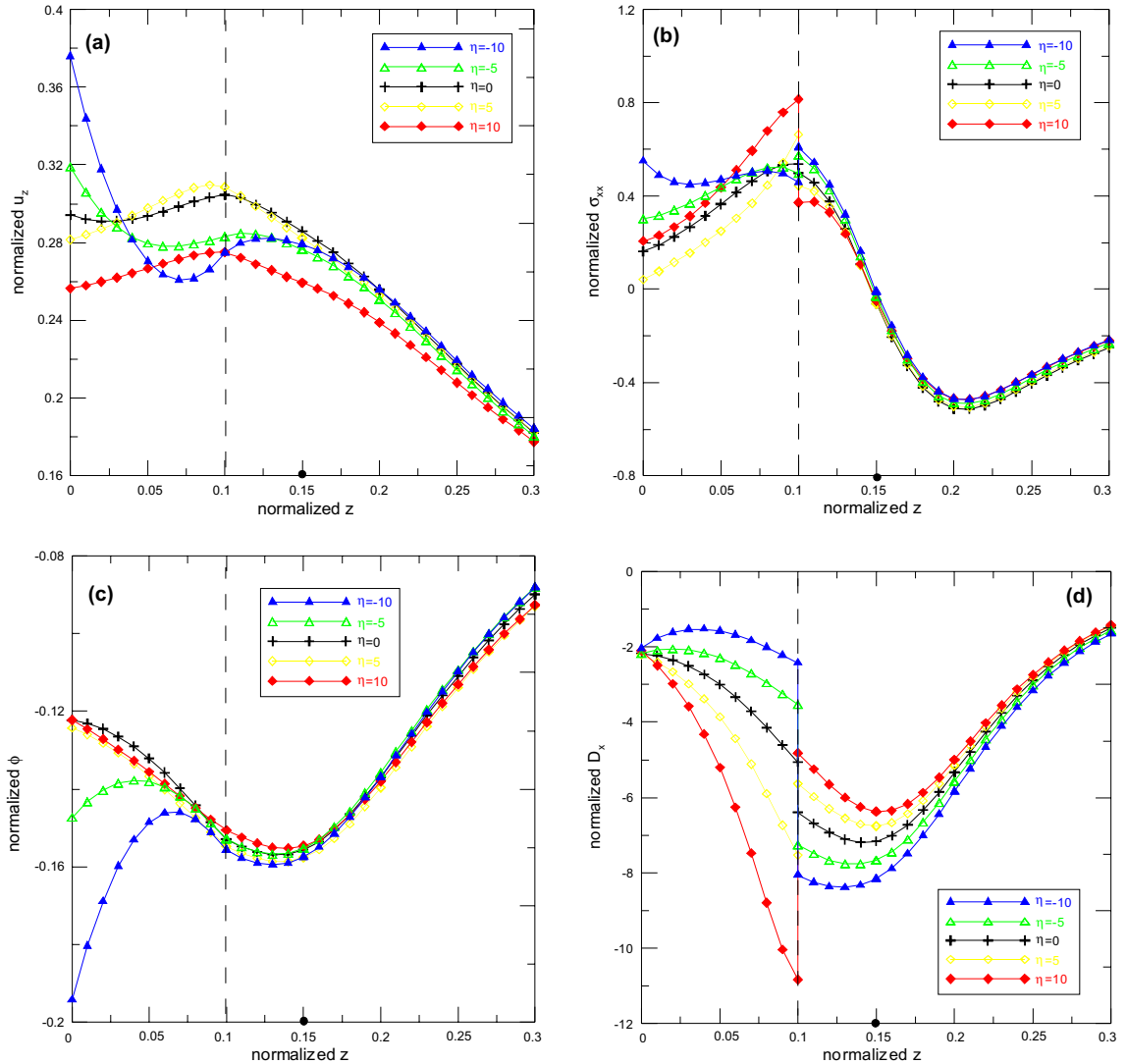
Fig. 11. Variation of the field quantities along a vertical line (from (0.1 m, 0, 0) to (0.1 m, 0, 0.3 m)) of the PFGM coated half space for the exponential factors $\eta = -10, -5, 0, 5,$ and 10, due to a negative point charge density Q of magnitude 1 C applied at (0, 0, 0.15 m). Elastic displacement component u_z in (a), stress component σ_{xx} in (b), electric potential ϕ in (c), and electric displacement component D_x in (d).

Figs. 11a–d show, respectively, the vertical elastic displacement u_z, horizontal stress component σ_{xx}, electric potential ϕ, and horizontal electric displacement D_x along the vertical line (from (0.1 m, 0, 0) to (0.1 m, 0, 0.3 m)) due to the negative point charge density of 1 C at (0.0, 0.0, 0.15 m). Similar to the responses due to the horizontal point force (Figs. 10a–d), the responses in the PFGM layer are substantially different for different exponential factors η. Furthermore, the responses in the underlying homogeneous half space can be also affected by the exponential factor in the PFGM layer (i.e., Figs. 11a and d). In contrast to the responses due to the point force, however, the slopes of the elastic and electric quantities are all continuous across the source point at $z = 0.15$ m.

8. Conclusions

In this paper, Green's functions for transversely isotropic PFGM and multilayered half spaces are derived, which include those for the corresponding elastic FGM media as the reduced case. By virtue of two systems of vector functions and the propagator matrix method, the Green's functions in the transformed domain are obtained in concise and unified forms. In order to find Green's functions in the physical-domain, which are expressed in one-dimensional infinite integrals with Bessel functions as integrands, we introduced and modified an adaptive Gauss quadrature. Green's function solutions are then applied to two PFGM models. One is the PFGM half space made of PZT-4 and the other is a PFGM coated half space where the coated PFGM layer is again PZT-4 and the underlying homogeneous half space is made of BaTiO$_3$. The influence of the exponential factor η of the PFGM is clearly demonstrated, and could be helpful to the future design and manufacturing of the PFGM structures. Although we discussed only the sources associated with the point force and point charge, the methodology presented in this paper could be extended to other concentrated sources such as dislocation, eigenstrain, etc. Implementation of the PFGM Green's functions to the boundary element program should also result in various interesting applications.

Acknowledgment

Appendix A. Cylindrical system of vector functions and associated source functions

The cylindrical system of vector functions is defined as (Pan, 1989a, 1997)

$$
\begin{aligned}
\boldsymbol{L}(r,\theta;\lambda,m) &= \boldsymbol{e}_z S(r,\theta;\lambda,m),\\
\boldsymbol{M}(r,\theta;\lambda,m) &= \left(\boldsymbol{e}_r\frac{\partial}{\partial r}+\boldsymbol{e}_\theta\frac{\partial}{r\partial\theta}\right)S(r,\theta;\lambda,m),\\
\boldsymbol{N}(r,\theta;\lambda,m) &= \left(\boldsymbol{e}_r\frac{\partial}{r\partial\theta}-\boldsymbol{e}_\theta\frac{\partial}{\partial r}\right)S(r,\theta;\lambda,m)
\end{aligned}
\tag{A.1}
$$

with

$$
S(r,\theta;\lambda,m)=\frac{1}{\sqrt{2\pi}}J_m(\lambda r)e^{im\theta},
\tag{A.2}
$$

where $J_m(\lambda r)$ is the Bessel function of order m with $m=0$ corresponding to the axial symmetric deformation.

The cylindrical system of vector functions is an extension of the Hankel transform and can be directly applied to a vector function. Since the cylindrical system (A.1) forms an orthogonal and complete space, any integrable vector and/scalar function can be expressed in terms of it. In particular, the elastic displacement vector, electric potential, traction vector, electric displacement vector, body force vector, and the negative charge density can be expressed as

$$
\boldsymbol{u}(r,\theta,\zeta)=\sum_m\int_0^{+\infty}[U_L(\zeta)\boldsymbol{L}(r,\theta)+U_M(\zeta)\boldsymbol{M}(r,\theta)+U_N(\zeta)\boldsymbol{N}(r,\theta)]\lambda\,\mathrm{d}\lambda,
\tag{A.3}
$$

$$
\phi(r,\theta,\zeta)=\sum_m\int_0^{+\infty}\Phi(\zeta)S(r,\theta)\lambda\,\mathrm{d}\lambda,
\tag{A.4}
$$

$$\boldsymbol{t}(r,\theta,\zeta) \equiv \sigma_{rz}\boldsymbol{e}_r + \sigma_{\theta z}\boldsymbol{e}_\theta + \sigma_{zz}\boldsymbol{e}_z = \sum_m \int_0^{+\infty} [T_L(\zeta)\boldsymbol{L}(r,\theta) + T_M(\zeta)\boldsymbol{M}(r,\theta) + T_N(\zeta)\boldsymbol{N}(r,\theta)]\lambda\,\mathrm{d}\lambda, \quad (A.5)$$

$$\boldsymbol{D}(r,\theta,\zeta) = \sum_m \int_0^{+\infty} [D_L(\zeta)\boldsymbol{L}(r,\theta) + D_M(\zeta)\boldsymbol{M}(r,\theta) + D_N(\zeta)\boldsymbol{N}(r,\theta)]\lambda\,\mathrm{d}\lambda, \quad (A.6)$$

$$\boldsymbol{f}(r,\theta,\zeta) = \sum_m \int_0^{+\infty} [F_L(\zeta)\boldsymbol{L}(r,\theta) + F_M(\zeta)\boldsymbol{M}(r,\theta) + F_N(\zeta)\boldsymbol{N}(r,\theta)]\lambda\,\mathrm{d}\lambda, \quad (A.7)$$

$$-q(r,\theta,\zeta) = \sum_m \int_0^{+\infty} Q(\zeta)S(r,\theta)\lambda\,\mathrm{d}\lambda. \quad (A.8)$$

Assume that there is a point force and a negative point charge density applied along the vertical axis in layer k at $z = d$ (or $\zeta = h_{k1}$), we then have, in the cylindrical coordinates,

$$f_j(r,\theta,\zeta) = \frac{\delta(r)\delta(\theta)\delta(\zeta - h_{k1})}{r} n_j, \quad (A.9)$$

$$-q(r,\theta,\zeta) = \frac{\delta(r)\delta(\theta)\delta(\zeta - h_{k1})}{r}, \quad (A.10)$$

where (n_x, n_y, n_z) are the (x, y, z)-direction cosines of the unite force vector in the space-fixed Cartesian coordinates, with x- and y-directions being taken, respectively, along $\theta = 0$ and $\theta = \pi/2$ of the cylindrical coordinates.

Substituting (A.9) and (A.10) into (A.7) and (A.8) respectively, one can show that the expansion coefficients of the point force and negative point charge density are, respectively

$$
\begin{aligned}
F_L &= \frac{n_z}{\sqrt{2\pi}}\delta(\zeta - h_{k1}); \quad m = 0, \\
F_M &= -\frac{\mp n_x + \mathrm{i}n_y}{2\lambda\sqrt{2\pi}}\delta(\zeta - h_{k1}); \quad m = \pm 1, \\
F_N &= -\frac{\mathrm{i}n_x \pm n_y}{2\lambda\sqrt{2\pi}}\delta(\zeta - h_{k1}); \quad m = \pm 1,
\end{aligned}
\quad (A.11)
$$

$$Q = \frac{-1}{\sqrt{2\pi}}\delta(\zeta - h_{k1}); \quad m = 0. \quad (A.12)$$

These point force and negative point charge density will cause the following discontinuities in the expansion coefficients of the traction vector and normal electric displacement component:

$$
\begin{aligned}
\Delta T_L &\equiv T_L(h_{k1} + 0) - T_L(h_{k1} - 0) = \frac{-n_z}{\sqrt{2\pi}}; \quad m = 0, \\
\Delta T_M &\equiv T_M(h_{k1} + 0) - T_M(h_{k1} - 0) = \frac{\mp n_x + \mathrm{i}n_y}{2\lambda\sqrt{2\pi}}; \quad m = \pm 1, \\
\Delta T_N &\equiv T_N(h_{k1} + 0) - T_N(h_{k1} - 0) = \frac{\mathrm{i}n_x \pm n_y}{2\lambda\sqrt{2\pi}}; \quad m = \pm 1,
\end{aligned}
\quad (A.13)
$$

$$\Delta D_L \equiv D_L(h_{k1} + 0) - D_L(h_{k1} - 0) = \frac{1}{\sqrt{2\pi}}; \quad m = 0. \quad (A.14)$$

Appendix B. Nonzero elements of coefficient matrix [A] in Eq. (3.24)

$$A_{12} = \lambda^2(\varepsilon_{33}^0 C_{13}^0 + e_{33}^0 e_{31}^0)/\Delta; \quad A_{13} = \varepsilon_{33}^0 e^{-\eta\zeta}/\Delta; \quad A_{16} = e_{33}^0 e^{-\eta\zeta}/\Delta;$$

$$A_{21} = -1; \quad A_{24} = e^{-\eta\zeta}/C_{44}^0; \quad A_{25} = -e_{15}^0/C_{44}^0; \quad A_{34} = \lambda^2;$$

$$A_{42} = \lambda^2\{C_{11}^0 - [C_{13}^0(\varepsilon_{33}^0 C_{13}^0 + e_{33}^0 e_{31}^0) + e_{31}^0(e_{33}^0 C_{13}^0 - C_{33}^0 e_{31}^0)]/\Delta\}e^{\eta\zeta};$$

$$A_{43} = -(\varepsilon_{33}^0 C_{13}^0 + e_{33}^0 e_{31}^0)/\Delta; \quad A_{46} = (e_{31}^0 C_{33}^0 - e_{33}^0 C_{13}^0)/\Delta;$$

$$A_{52} = \lambda^2(e_{33}^0 C_{13}^0 - C_{33}^0 e_{31}^0)/\Delta; \quad A_{53} = e_{33}^0 e^{-\eta\zeta}/\Delta; \quad A_{56} = -C_{33}^0 e^{-\eta\zeta}/\Delta;$$

$$A_{64} = \lambda^2 e_{15}^0/C_{44}^0; \quad A_{65} = -\lambda^2(\varepsilon_{11}^0 + (e_{15}^0)^2/C_{44}^0)e^{-\eta\zeta},$$

$$\tag{B.1}$$

where

$$\Delta = (e_{33}^0)^2 + C_{33}^0\varepsilon_{33}^0. \tag{B.2}$$

Appendix C. Nonzero elements of coefficients matrix [W] in Eq. (3.26)

$$W_{12} = (\varepsilon_{33}^0 C_{13}^0 + e_{33}^0 e_{31}^0)/\Delta; \quad W_{13} = \varepsilon_{33}^0/\Delta; \quad W_{16} = e_{33}^0/\Delta;$$

$$W_{21} = -1; \quad W_{24} = 1/C_{44}^0; \quad W_{25} = -e_{15}^0/C_{44}^0; \quad W_{33} = -\eta/\lambda; \quad W_{34} = 1;$$

$$W_{42} = C_{11}^0 - [C_{13}^0(\varepsilon_{33}^0 C_{13}^0 + e_{33}^0 e_{31}^0) + e_{31}^0(e_{33}^0 C_{13}^0 - C_{33}^0 e_{31}^0)]/\Delta;$$

$$W_{43} = -(\varepsilon_{33}^0 C_{13}^0 + e_{33}^0 e_{31}^0)/\Delta; \quad W_{44} = -\eta/\lambda; \quad W_{46} = (e_{31}^0 C_{33}^0 - e_{33}^0 C_{13}^0)/\Delta;$$

$$W_{52} = (e_{33}^0 C_{13}^0 - C_{33}^0 e_{31}^0)/\Delta; \quad W_{53} = e_{33}^0/\Delta; \quad W_{56} = -C_{33}^0/\Delta;$$

$$W_{64} = e_{15}^0/C_{44}^0; \quad W_{65} = -(\varepsilon_{11}^0 + (e_{15}^0)^2/C_{44}^0); \quad W_{66} = -\eta/\lambda,$$

$$\tag{C.1}$$

where

$$\Delta = (e_{33}^0)^2 + C_{33}^0\varepsilon_{33}^0. \tag{C.2}$$

Appendix D. Material properties of PZT-4 and BaTiO$_3$

For the PZT-4, the elastic, piezoelectric, and dielectric coefficient matrices are respectively (Pan et al., 2001)

$$[C^0] = \begin{bmatrix} 1.39 & 0.778 & 0.743 & 0 & 0 & 0 \\ 0.778 & 1.39 & 0.743 & 0 & 0 & 0 \\ 0.743 & 0.743 & 1.15 & 0 & 0 & 0 \\ 0 & 0 & 0 & 0.256 & 0 & 0 \\ 0 & 0 & 0 & 0 & 0.256 & 0 \\ 0 & 0 & 0 & 0 & 0 & 0.306 \end{bmatrix} (10^{11} \text{ N/m}^2), \tag{D.1}$$

$$[e^0] = \begin{bmatrix} 0 & 0 & 0 & 0 & 12.7 & 0 \\ 0 & 0 & 0 & 12.7 & 0 & 0 \\ -5.2 & -5.2 & 15.1 & 0 & 0 & 0 \end{bmatrix} \ (\text{C/m}^2), \tag{D.2}$$

$$[\varepsilon^0] = \begin{bmatrix} 0.64605 & 0 & 0 \\ 0 & 0.64605 & 0 \\ 0 & 0 & 0.561975 \end{bmatrix} \ (10^{-8} \ \text{CV}^{-1} \ \text{m}^{-1}), \tag{D.3}$$

and for $BaTiO_3$, they are (Pan et al., 2001)

$$[C^0] = \begin{bmatrix} 1.66 & 0.77 & 0.78 & 0 & 0 & 0 \\ 0.77 & 1.66 & 0.78 & 0 & 0 & 0 \\ 0.78 & 0.78 & 1.62 & 0 & 0 & 0 \\ 0 & 0 & 0 & 0.43 & 0 & 0 \\ 0 & 0 & 0 & 0 & 0.43 & 0 \\ 0 & 0 & 0 & 0 & 0 & 0.445 \end{bmatrix} \ (10^{11} \ \text{N/m}^2), \tag{D.4}$$

$$[e^0] = \begin{bmatrix} 0 & 0 & 0 & 0 & 11.6 & 0 \\ 0 & 0 & 0 & 11.6 & 0 & 0 \\ -4.4 & -4.4 & 18.6 & 0 & 0 & 0 \end{bmatrix} \ (\text{C/m}^2), \tag{D.5}$$

$$[\varepsilon^0] = \begin{bmatrix} 1.12 & 0 & 0 \\ 0 & 1.12 & 0 \\ 0 & 0 & 1.26 \end{bmatrix} \ (10^{-8} \ \text{CV}^{-1} \ \text{m}^{-1}). \tag{D.6}$$

References

Almajid, A.A., Taya, M., Hudnut, S., 2001. Analysis of out-of-plane displacement and stress field in a piezocomposite plate with functionally graded microstructure. Int. J. Solids Struct. 38, 3377–3391.

Almajid, A.A., Taya, M., 2001. 2D-elasticity of FGM piezo-laminates under cylindrical bending. J. Intel. Mat. Syst. Struct. 12, 341–351.

Berger, J.R., Martin, P.A., Mantic, V., Gray, L.J., in press. Fundamental solutions for steady-state heat transfer in an exponentially graded anisotropic material. Z. Angew. Math. Phys.

Chan, Y.-S., Gray, L.J., Kaplan, T., Paulino, G.H., 2004. Green's functions for a two-dimensional exponentially-graded elastic medium. Proc. R. Soc. Lond. A 460, 1689–1706.

Chave, A.D., 1983. Numerical integration of related Hankel transforms by quadrature and continued fraction expansion. Geophysics 48, 1671–1686.

Chen, Y.H., Ma, J., 2002. Electrophoretic deposition and characterization of FGM piezoelectric monomorph actuator. In: Proceedings of the Second International Conference on Advanced Materials Processing, pp. 487–490.

Dunn, M.L., Taya, M., 1993. An analysis of piezoelectric composite materials containing ellipsoidal inhomogeneities. Proc. R. Soc. Lond. A 443, 265–287.

Giannakopoulos, A.E., Suresh, S., 1997. Indentation of solids with gradients in elastic properties: Part I. Point force. Int. J. Solids Struct. 34, 2357–2392.

Giannakopoulos, A.E., Suresh, S., 1999. Theory of indentation of piezoelectric materials. Acta Mater. 47, 2153–2164.

Gilbert, F., Backus, G., 1966. Propagator matrices in elastic wave and vibration problems. Geophysics 31, 326–332.

Gray, L.J., Kaplan, T., Richardson, J.D., Paulino, G.H., 2003. Green's functions and boundary integral analysis for exponentially graded materials: heat conduction. J. Appl. Mech. 70, 543–549.

Hirai, T., 1995. Functional gradient materials. Materials Science and Technology: A Comprehensive Treatment, Processing of Ceramics, vol. 17B, Part 2. Wiley, New York, pp. 292–341.

Jarvis, E.A., Carter, E.A., 2002. The role of reactive elements in thermal barrier coatings. Comput. Sci. Eng. 4, 33–41.

Kim, J.H., Paulino, G.H., 2002a. Mixed-mode fracture of orthotropic functionally graded materials using the finite elements and the modified crack closure method. Eng. Fract. Mech. 69, 1557–1586.

Kim, J.H., Paulino, G.H., 2002b. Isoparametric graded finite elements for nonhomogeneous isotropic and orthotropic materials. J. Appl. Mech. 69, 502–514.

Kim, J.H., Paulino, G.H., 2003. An accurate scheme for mixed-mode fracture analysis of functionally graded materials using the interaction integral and micromechanics models. Int. J. Numer. Methods Eng. 58, 1457–1497.

Liew, K.M., Yang, J., Kitipronchai, S., 2003. Postbuckling of piezoelectric FGM plates subject to thermo-electro-mechanical loading. Int. J. Solids Struct. 40, 3869–3892.

Lucas, S.K., 1995. Evaluating infinite integrals involving products of Bessel functions of arbitrary order. J. Comput. Appl. Math. 64, 269–282.

Markworth, A.J., Ramesh, K.S., Parks Jr., W.P., 1995. Modelling studies applied to functionally graded materials. J. Mater. Sci. 30, 2183–2193.

Martin, P.A., Richardson, J.D., Gray, L.J., Berger, J.R., 2002. On Green's function for a three-dimensional exponentially graded elastic solid. Proc. R. Soc. Lond. A 458, 1931–1947.

Miyamoto, Y., Kaysser, W.A., Rabin, B.H., Kawasaki, A., Ford, R.G., 1999. Functionally Graded Materials: Design, Processing and Applications. Kluwer Academic Publishers, Dordrecht.

Newnham, R.E., Amin, A., 1999. Smart systems: Microphones, fish farming, and beyond-Smart materials, acting as both sensors and actuators, can mimic biological behavior. Chem. Tech. 29, 38–46.

Pan, E., 1989a. Static response of a transversely isotropic and layered half-space to general surface loads. Phys. Earth Planet. Inter. 54, 353–363.

Pan, E., 1989b. Static response of a transversely isotropic and layered half-space to general dislocation sources. Phys. Earth Planet. Inter. 58, 103–117.

Pan, E., 1997. Static Green's functions in multilayered half spaces. Appl. Math. Modell. 21, 509–521.

Pan, E., 1999. Green's function in layered poroelastic half-space. Int. J. Numer. Anal. Methods Geomech. 23, 1631–1653.

Pan, E., Yang, B., Cai, G., Yuan, F.G., 2001. Stress analysis around holes in composite laminates using boundary element method. Eng. Anal. Bound. Elements 25, 31–40.

Pan, E., 2002. Mindlin's problem for an anisotropic piezoelectric half space with general boundary conditions. Proc. R. Soc. Lond. A 458, 181–208.

Pan, E., Han, F., 2004. Green's functions for transversely isotropic piezoelectric multilayered half-spaces. J. Eng. Math. 49, 271–288.

Rodel, J. (Ed.), 2003. Priority Program: Functionally Graded Materials (1995–2002). In: Materials Science & Engineering, vol. A362, Special Issue Nos. 12.

Santare, M.H., Thamburaj, P., Gazonas, G.A., 2003. The use of graded finite elements in the study of elastic wave propagation in continuously nonhomogeneous materials. Int. J. Solids Struct. 40, 5621–5634.

Suresh, S., Mortensen, A., 1998. Fundamentals of Functionally Graded Materials. Institute of Materials, London.

Sutradhar, A., Paulino, G.H., Gray, L.J., 2002. Transient heat conduction in homogeneous and non-homogeneous materials by the Laplace transform Galerkin boundary element method. Eng. Anal. Bound. Elements 26, 119–132.

Wang, C.D., Tzeng, C.S., Pan, E., Liao, J.J., 2003. Displacements and stresses due to a vertical point load in an inhomogeneous transversely isotropic half-space. Int. J. Rock Mech. Min. Sci. 40, 667–685.

Xu, J., Zhu, X., Meng, Z., 1999. Effect of the interdiffusion reaction on the compatibility of PZT/PNN functionally gradient piezoelectric materials. IEEE Transactions on Components and Packaging Technology 22, 11–16.

Yang, J.S., Tiersten, H.F., 1997. Elastic analysis of the transfer of shearing stress from partially electroded piezoelectric actuators to composite plates in cylindrical bending. Smart Mater. Struct. 6, 333–340.

Yue, Z.Q., Yin, J.H., 1998. Backward transfer-matrix method for elastic analysis of layered solids with imperfect bonding. J. Elasticity 50, 109–128.